AEDC-TDR-62-218

MEASUREMENTS OF PRESSURE AND SPEED OF FLOW IN A SPARK-HEATED HYPERSONIC WIND TUNNEL

By

Krishnamurty Karamcheti, Walter Vali,

James B. Kyser, and Maurice L. Rasmussen

Department of Aeronautics and Astronautics

Stanford University

Stanford California

(The reproducible copy supplied by the authors was used in the reproduction of this report.)

November 1962

AF - AEDC
Arnold AFS Tenn

ABSTRACT

An account is given of several aspects of the experimental investigation directed at determining the nature of the flow and state of the gas in the nozzle and test section of the Stanford spark-heated hypersonic wind tunnel. Attention is given only to the pressure and speed-of-flow measurements. Results are presented for pitot pressures and wall static pressures.

The speed of flow in the test section is derived from measurements made by spark-schlieren photographs of a disturbance created in the flow by means of a spark discharge. On the basis of these measurements, it is concluded that the actual stagnation enthalpy of the stream is likely to be different from the enthalpy calculated according to current practice. As a consequence, it is shown that serious errors may occur in the calculated values for the state of the flow, and in theoretical estimates of quantities such as stagnation-point heat-transfer rates.

CONTENTS

ILLUSTRATIONS

NOMENCLATURE

A_*	Area of throat
A_e/A_*	Effective area ratio
A_G/A_*	Geometric area ratio
a	Speed of sound
d	Displacement of a disturbance in the test section
h	Enthalpy
M	Mach number
n	Factor defined by $1 - (h/h_o)$
p	Pressure
q	Dynamic pressure
$\dot{q}_a$	Aerodynamic heat-transfer rate
$\dot{q}_p$	Particle-induced heat-transfer rate
$\dot{q}_{th}$	Theoretical stagnation-point heat-transfer rate
R	Gas constant
R_e	Reynolds number
r	Density ratio across normal shock wave, ρ/ρ_2
r_w	radius of the disturbance wave
T	Temperature
t	Time
V	Longitudinal flow velocity
w	Abbreviation of $(1/4)\ M_2^2$
Z	Compressibility factor
α	Abbreviation for $(r_c/r_m)^{0.25}$
μ	Viscosity
ρ	Density
σ	Ratio of particle density to gas density

NOMENCLATURE (Cont'd)

Subscripts

o	Relates to reservoir conditions
2	Condition just after a normal shock
c	Values of quantities deduced on the basis of measured pressures p_o and p_s
m	Values of quantities deduced on the basis of measured velocity V and measured pressure p_s
s	Stagnation condition behind a normal shock
w	relates to disturbance wave

1.0 INTRODUCTION

The Department of Aeronautics and Astronautics at Stanford University has been concerned with an investigation of the basic performance of a spark-heated hypersonic wind tunnel, the so-called hotshot tunnel. The investigation has included both experimental and analytical work and is directed at determining the nature of the flow and the state of the gas in the nozzle and the test section of such a tunnel. Some aspects of the experimental work form the contents of this report. The analytical work is covered by Vincenti (1961) and Emanuel and Vincenti (1962).

As a first step in the experimental program a capacitance-driven spark-heated hypersonic wind tunnel was designed, built and put into operation in 1959. Thereafter, efforts have been directed at obtaining reliable measurements of the state (static and pitot pressure, speed, speed of sound) of the flow in the test section. The purpose of this report is to describe briefly the wind tunnel and measuring techniques, to present the measurements, and to discuss the results thus obtained.

In view of the special problems associated with flows of large stagnation enthalpy, such as those occurring in a hotshot tunnel, one of the aims of the experimental program has been to explore the possibilities of measuring a number of independent quantities in the flow. If a sufficient number of such quantities is measured, one may hope to evaluate the state of the test-section stream without the aid of special assumptions regarding the flow through the nozzle. This is a necessary step in the proper utilization of a facility involving large stagnation enthalpies and any associated nonequilibrium effects when they occur. Accordingly, besides the usual measurements of pitot and static pressure, attempts have been made to measure the speed of flow, the speed of sound in the stream and the temperature of the stream, and the level of contamination in the stream due to solid particles arising out of the processes in the arc chamber. The measurements of pitot and static pressure follow conventional techniques. The speed of flow and the speed of sound are to be measured by means of schlieren pictures of the rate of displacement and growth of a disturbance produced by a spark discharge in the gas stream. The temperature and the level of contamination are to be measured by means of a two-color pyrometer which measures the temperature of the solid contaminants in the stream. In this report, attention is given only to the pressure and speed-of-flow measurements. For information on the pyrometer measurements reference may be made to Karamcheti et al.(1962) and Vali and deVoto (1962).

The speed-of-flow measurements have shown, as discussed in detail later, that the enthalpy in the arc chamber computed according to present practice (see section 3.0) may, in general, be in considerable error and that as a consequence the calculated values for the flow conditions in the test section are also in error. This aspect was pointed out originally by Karamcheti et al. (1962) at the Second Symposium on Hypervelocity Techniques.

The authors are indebted to Messrs. Denis Tsao and David Greenberg for their assistance in carrying out the experimental program. Special thanks are also due to Professor Walter G. Vincenti for many valuable discussions.

2.0 STANFORD SPARK-HEATED HYPERSONIC WIND TUNNEL

2.1 GENERAL CONSIDERATIONS

The Stanford spark-heated tunnel is of the so-called "hotshot" type. It is similar in its essential features to the Hot Shot I tunnel (designated as AEDC-16) at the Arnold Engineering Development Center. For information on the AEDC-16 tunnel, reference may be made to Lukasiewicz et al. (1960).

The Stanford Tunnel consists of an arc chamber, a hypersonic nozzle and test section, a diffuser, and a vacuum tank. The general features are shown in Figures 1 and 2. It was the intention to provide maximum operating conditions of 20,000 psi and 8000°K in the arc chamber immediately after energy discharge.

2.2 ENERGY STORAGE AND DISCHARGE SYSTEM

2.2.1 Energy Storage

The energy storage for the tunnel is in a capacitor bank of 138, 81-microfarad General Electric capacitors with a maximum voltage of 6,000 volts. The maximum energy storage is thus 200,000 joules. Three of the capacitors are used to provide the energy to explode the trigger wire that initiates the main discharge. The capacitors are charged by a constant-current power supply that requires approximately two minutes to bring the bank to full voltage.

The energy transmission from the capacitor bank to the arc chamber is by means of a parallel system of 15-foot-long coaxial cables running from each capacitor to a collector assembly on the rear of the arc chamber. The collector assembly, which consists of a set of cylindrical discs, connects directly to the back end of the arc chamber and to the main electrode as shown in Figure 3. The axis of the collector coincides with the axes of the electrodes and the arc chamber, thus insuring that the entire electrical path is coaxial. Each collector disc is made up of two concentric copper rings (forming the two parts of the coaxial path) separated by plexiglass spacers. The individual cables from the capacitors are connected radially to the copper rings. The total inductance of the energy storage system is about 1/4 microhenry.

2.2.2 Discharge Characteristics

During the discharge of energy, measurements were made of the variation with time of the voltage $V(t)$, the current $i(t)$ and the rate of change of the current di/dt. Integration of the di/dt curve yields a current-versus-time curve which is then used to check the measured $i(t)$. The agreement between the two, for several tests, was found to be satisfactory.

Typical voltage and current curves as obtained in two runs of the tunnel are shown in (a) and (b) of Figure 4. The measurements indicate that the discharge is nearly critically damped and that the time of discharge is about 100 microseconds.

From the measured values of the voltage and current, the resistance R_a of the arc as a function of time was computed approximately from the formula

$$R_a(t) = \frac{V(t)}{i(t)}$$

which neglects the inductance of the arc chamber. It has been estimated that the inductance would change the calculated resistance by less than a factor of two. The arc resistance, thus computed, is presented in (c) of Figure 4. It is seen that the resistance is nearly constant during the discharge.

2.3 ARC CHAMBER

The general features of the arc chamber are shown in Figure 3 which is self-explanatory. The free volume of the arc chamber can be varied from 22 to 26 cubic inches. During the tests, two electrode configurations, as shown in Figure 5, were used. In both configurations, the main (i.e., high-voltage) electrode is brought in centrally through the rear of the chamber. The difference between the configurations is in the way the return electrical path is provided. In the configuration shown in (a) of Figure 5 (also c.f. Fig. 3) the return (or ground) electrode, being on the same axis as the main electrode, is supported by four spokes from a cylindrical sleeve that is concentric with the chamber. The electrodes thus face each other and we shall refer to this configuration as "with facing electrodes". In the other electrode configuration, shown in (b) of Figure 5, there is no ground electrode as such, the entire inner surface of the chamber acting as the electrode. We shall refer to this as the configuration "without facing electrodes".

2.4 NOZZLE, TEST SECTION, AND DIFFUSER

The main features of the nozzle, test section and diffuser are shown in Figure 6. The nozzle, which is a simple cone of 8° 20' included angle, is approximately 130 inches long. The first part of the nozzle

containing the throat is shown in Figure 3. The final 24 inches of the nozzle forms the test section. The exit diameter of the test section is 18.9 inches. Glass windows (8 inches in diameter) for schlieren photography, and mounting ports for the disturbance electrodes (see section 5.2) are provided in the test section. Flush aluminum inserts to replace the glass windows are also available. The nozzle and arc chamber are mounted on wheels so as to allow easy access to the test section.

Following the test section is a 10-inch-long cylindrical instrumentation section. This section contains model and/or probe mountings and provides access for the instrumentation leads. For the measurements reported here, the pitot probe is mounted on a sharp-edged strut-and-sting assembly.

A diffuser, which is a simple cone-cylinder, follows the instrumentation section (see Fig. 6). The conical portion of the diffuser is 43 inches long with an included angle of 8° 20'. It is followed by a 12.6 inch diameter cylindrical section, 36 inches long. This choice of diffuser configuration was made on the basis of several tests carried out with different diffusers. The objective was to achieve, under the present conditions of operation (see page 57), a long running time, about 30 milliseconds of quasi-steady flow through the nozzle and over the probe. Without the use of the present diffuser it was not possible to obtain running times over 5 milliseconds.

2.5 VACUUM TANK AND VACUUM EQUIPMENT

The vacuum tank (or chamber) is 23 inches in inside diameter and 12 feet long. The diffuser (c.f., Fig. 6) extends into the vacuum chamber for 79 inches, thus occupying about 55 percent of the length of the tank.

The vacuum equipment consists of a mechanical pump with a capacity of about 50 cu ft per minute, a diffusion-ejector pump, with a speed of about 320 liters per sec. at 1 micron Hg, and a set of Pirani vacuum gauges. The nozzle, the test section, and the vacuum tank can together be pumped down from atmospheric pressure to one micron of mercury in less than 30 minutes.

2.6 TEST CONDITIONS

All of the measurements reported here were made, using nitrogen gas, at nominal initial conditions in the arc chamber immediately after energy discharge of 4000°K temperature and 10,000 psi pressure. The nominal computed Mach number in the test section is about 17; the computed density in the test section is about one-thousandth of atmospheric density (0.00242 slugs per cu ft). The running time consisting of quasi-steady flow in the test section is about 30 milliseconds.

3.0 CALCULATION OF FLOW CONDITIONS

The flow conditions in the tunnel are calculated generally according to the method reported by Grabau et al. (1961). The method utilizes the following measured quantities as the basic input data:

(1) the pressure in the arc chamber before discharge, (2) the temperature of the gas in the chamber before discharge, (3) the time history of the arc-chamber pressure $p_o(t)$, and (4) the time history of the pitot pressure $p_s(t)$ in the test section. The method of calculation is built up on the following basic assumptions:

(1) the flow, though time dependent, is quasi-steady;

(2) the conditions in the arc chamber at every instant are uniform and correspond to thermodynamic equilibrium;

(3) the inviscid core of the flow through the nozzle is one-dimensional, adibiatic, equilibrium flow; and,

(4) the Mach number of the flow in the test section is equal to or greater than 10.

The two main steps in the calculations are as follows:

(1) On the basis of the measured pressure and temperature in the arc chamber before discharge together with the measured time history of the arc-chamber pressure $p_o(t)$, the time variation of other thermodynamic quantities such as the enthalpy, entropy, temperature, etc., of the gas in the arc chamber are computed.

(2) Using the arc-chamber enthalpy and entropy thus computed and the measured pitot pressure $p_s(t)$ in the test section, calculations are made of all other desired flow quantities in test-section stream or behind a normal shock in the test section. The equations necessary for the calculations are developed on the basis of normal shock relations and the compressible Bernoulli equation for the flow behind the shock.

The actual computation of the flow conditions is routinely carried out on a Burroughs 220 computer.

4.0 PRESSURE MEASUREMENTS

4.1. PRESSURE INSTRUMENTATION

Measurements of arc-chamber pressure are made with a commercially available (Norwood) unbonded strain-gage transducer and with a bonded strain-gage transducer designed and fabricated at Stanford. The range of these transducers is 0-20,000 psi. For the pitot and static pressures, commercially available (Hidyne) variable-reluctance transducers in the range of 0-5 psi and 0-0.5 psi differential are employed. The

performance of these transducers is described by Mulkey et al. (1958) and by Earheart and Bynum (1960). The transducers are used in conjunction with 20-kilocycle carrier-amplifier equipment (CEC) and the output is recorded on a commercial recording oscillograph (CEC). The recording galvanometers are flat to 1000 cps in the case of the arc-chamber pressures and to 185 cps in the case of the static and pitot pressures. The initial pressure in the arc chamber before discharge is measured by means of a Heise pressure gauge with a maximum range of 1,000 psi and an accuracy of ± 1/2 psi.

The calibration of the pressure transducers is made statically before every run. The arc-chamber transducers are calibrated with reference to a Heise 30,000 psi bourdon-type pressure gauge. The transducers for the static and pitot pressures are calibrated by means of U-tube manometers using oil of unit specific gravity (for low pressures) and mercury (for high pressures). The static-pressure transducers are usually calibrated in the range 0 to 15 mm Hg. Calibration in the range 0 to 1 mm Hg is periodically checked with reference to McLeod and Alphatron gages.

Typical oscillograph records of the pressures measured during a run of the tunnel are shown in Figure 7. It is seen that quasi-steady flow occurs for about 25-30 milliseconds. The initial transient occupies the first 8-10 milliseconds.

4.2 ARC-CHAMBER PRESSURE

Typical records of the arc-chamber pressure for ten runs are shown in Figure 8. All the runs shown are carried out, as mentioned before, at the same nominal initial conditions. It is seen that the peak pressure (i.e., that occurring immediately after energy discharge) is in the range of 9,300-10,300 psi. The measured data indicate that even for equal input conditions to the arc chamber, differences exist in the arc-chamber pressures from run to run. Although repeatability of data for the same nominal initial conditions is highly desirable, it is not clear at the present time whether the lack of it is a serious drawback in the proper utilization of a hotshot-type wind tunnel. It appears (see section 5.4) that what is required in this direction is the simultaneous measurement of as many flow quantities as required to determine locally the state of the flow.

In order to see how the decay of pressure in the arc chamber correlates from one run to another, the arc-chamber pressures shown in Figure 8 are replotted in a normalized form in Figure 9. For each run, the pressure occurring at 4 milliseconds in that run is chosen as the reference pressure. One can choose the peak pressure as the reference pressure, but it is rather hard to measure it unambiguously from the oscillograph records. It is seen that from run to run there is better agreement between the normalized curves of the pressure decay in the arc chamber than between the curves of the absolute pressure.

4.3 PITOT PRESSURE

The pitot pressure in the test section is measured by means of a 1.5-inch-diameter hemisphere-cylinder probe located at 117 inches from the throat. Figure 10 shows, for ten nominally identical runs, the time history of the pitot pressure. The transient state which occupies about the first 8 milliseconds is not shown. The pitot pressures are in the range of 0.4 psi to 1.5 psi.

Figure 11 shows, for the same runs, the ratio of the arc-chamber pressure at any instant to the pitot pressure at that instant as a function of time. Generally, for a given run, this ratio is nearly constant with time during the quasi-steady part of the flow.

4.4 STATIC PRESSURE ON NOZZLE WALL

Measurements of the time history of the static pressure at selected points on the wall on the nozzle are routinely made to monitor the conditions of the flow in the tunnel. For the present tests, measurements were made at stations 96, 113.5 and 125.5 inches from the throat. The location of the static-pressure taps is shown in Fig. 6.

To see the influence of the pitot probe on the pressure distribution along the nozzle wall, measurements of the wall pressure were made for the following three different situations: (i) tunnel empty, (ii) with a 1.5-inch hemisphere-cylinder pitot probe located on the tunnel centerline at 117 inches from the throat, and (iii) with a pitot probe consisting of a 2.75-inch-diameter disc (normal to the axis of the probe) located on the centerline at 117 inches from the throat. Figure 12 shows for these three situations the distribution of wall pressure at 20 milliseconds from the instant of arc discharge. (The tests were made, as mentioned before, at the same nominal initial conditions). It is seen that both with the tunnel empty and with the hemisphere-cylinder probe present, the wall pressures show a negative gradient along the nozzle. With the disc pitot probe, however, the pressures increase by a considerable amount downstream of the station 96 inches from the throat. Compared with the pressures measured when the tunnel is empty, the pressures occurring in the presence of the hemisphere-cylinder probe in the tunnel are slightly greater but, as is seen, only downstream of the station 113.5 inches from the throat. The probe, it may be recalled, is located at 117 inches. These observations show the influence on the pressure distribution along the wall of the interaction of the shock wave from the pitot probe with the wall boundary layer. As one would expect, the effect of the interaction is stronger for the disc probe than for the hemisphere-cylinder probe. On the basis of these observations, the present choice of the size and location of the hemisphere-cylinder pitot probe may be considered satisfactory from the point of view of its negligible effect on the pressure distribution along the wall in the test section.

To look further into the implications of the effect of the interaction resulting from the presence of the pitot probe, comparison is made between the measured wall pressures and calculated values for the static pressure in the test-section stream. The stream static pressure is computed, following Grabau et al. (1961), on the basis of the measured pitot and arc-chamber pressures. Since the pitot probe is located at 117 inches from the throat, the computed static pressure corresponds to approximately that location. Calculated values of the static pressure are included in Figure 12. It is seen that in the presence of the hemisphere-cylinder probe, the calculated values for the stream static pressure and those indicated by the measured wall pressures are in fair agreement. In the presence of the disc probe, there is no agreement between the wall pressure and the calculated value. The calculated values in this case, however, compare favorably with those computed and measured in the presence of the hemisphere-cylinder probe. This indicates that the shock-wave boundary-layer interaction resulting from the presence of the probe which seriously affects the pressure distribution on the nozzle wall, seems to have practically no effect on the static pressure in the stream. The flow at the probe is actually influenced by that portion of the nozzle which is upstream of the probe and bounded by the upstream-running characteristics from the probe. It follows, therefore, that the interaction between the shock wave from the probe and the boundary layer on the nozzle wall does not extend up to the position of the nozzle that actually influences the flow at the probe.

The wall pressures vary during a run and from run to run. A qualitative plot giving the range of variation in ten nominally identical runs is shown in Figure 13. Also included in the figure is the range of calculated values, for the same runs, of the static pressure in the stream.

5.0 SPEED-OF-FLOW MEASUREMENTS

5.1 PRINCIPLE

The measurement of the speed of flow and the speed of sound in the test-section stream is based on the following simple considerations. If, in a uniform stream of speed V, at a certain instant of time, an acoustic disturbance, say a spherical or cylindrical wave is created, then in time Δt the disturbance as a whole is displaced through a distance

$$d = V\Delta t$$

in the direction of the stream, while it grows into a sphere or cylinder of radius

$$r_w = a\Delta t$$

where a is the speed of sound in the flow. The speeds V and a are assumed uniform. These two relations serve to determine V and a, if one measures d, r_w and Δt. The displacement d and the radius r_w can be measured from a schlieren photograph of the disturbance taken at the end of the time interval Δt, while Δt can be measured by electronic instrumentation.

When the disturbance is not an acoustic wave, the speed of propagation of the disturbance relative to the stream is no longer the speed of sound. In such a case it is not possible to derive the speed of sound in the flow from the measurements described; however, the speed of flow can still be obtained by measuring d and Δt. At the conditions of flow existing in the present investigations, the disturbance could not be made an acoustic wave and yet be detected by the schlieren system. Therefore, the present measurements were used to deduce the speed of flow only.

The foregoing method has been used previously by Elliot (1955) to measure the speed of flow in a conventional supersonic tunnel. Cunningham and Kraus (1958) also used the method at hypersonic speeds. Cox (1959) and Merritt (1961) reported the use of the same technique for measuring the flow speed in a hypersonic gun tunnel.

5.2 DESCRIPTION OF APPARATUS

The apparatus necessary for the schlieren measurements consists of the following major components: (1) the schlieren optics, (2) the disturbance-spark system, (3) the time-delay system to provide the necessary time intervals between the starting of the tunnel and the creating of the disturbance spark and the triggering of the light source of the schlieren system, (4) the time-measuring unit to measure the time interval Δt between the disturbance spark and schlieren spark. A general layout of the complete system is shown in Figure 14. Considerations underlying the design of the apparatus, a description of the apparatus, and a discussion of the performance of the system have been given by Thomas (1961). Some of the salient features are as follows:

The schlieren unit consists of a double-pass schlieren system, as shown schematically in Figure 15. The system has a 10-ft-focal-length, 10-inch-diameter spherical mirror and a short-duration-spark light source. The spark gap is located coaxially with and at the center of a low-inductance annular capacitor. For a general discussion on the design and setting up of schlieren systems, reference may be made to Holder and North (1956).

The disturbance is created by discharging a $0.1\mu F$, 8KV capacitor between the tips of two electrodes mounted in the test section (see Figure 16). The gap between the electrode tips is set at 4 inches so as to provide a cylindrical disturbance. Such an arrangement, suggested by Merritt (1961), has been found to be free of the effects of the wake

from the electrodes and to be more suitable for schlieren photography than a spherical disturbance. The electrodes can be mounted so that the axis of the disturbance is normal to the direction of flow in the tunnel and is either parallel or normal to the axis of the schlieren system. The electrodes are made of 1/8-inch-diameter steel drill rod and are insulated over their entire length except for the tips.

In operation, the disturbance is set off in the upstream portion of the test section at a time anywhere from 2 to 35 milliseconds after the discharge of energy into the arc chamber. Following this, the schlieren spark is triggered at any instant in the range from 2 to 60 microseconds later, and a photograph is obtained of the disturbance as it traverses the test section.

The electronic circuits include those needed for the following: disturbance spark, schlieren spark, delay units, and unit to measure time interval. The disturbance-spark circuit is shown in Figure 17. The schlieren-spark circuit is essentially similar. The schlieren spark is initiated by discharging a trigger capacitor in the spark gap and thereby ionizing the gap. The discharge of the trigger capacitor is effected by a thyratron. The disturbance spark is triggered directly by means of a thyratron.

The desired time intervals are provided by means of Techtronix 160-Series wave-form generator, pulse generator, and power supply. The measurement of the time interval Δt is made by means of a Beckman Universal EPUT and Timer.

5.3 RESULTS

Schlieren photographs of a disturbance with no flow in the tunnel have been obtained at densities corresponding to pressures as low as 100 microns Hg at room temperature (the wave, of course, is not acoustic). This is significant in the sense that a density corresponding to 1000 microns Hg at room temperature is usually considered the limit of sensitivity of a schlieren system.

Figure 18 shows the shape of the disturbance wave. In (a) the disturbance is viewed along its axis with no flow in the tunnel. In (b) a similar view is shown with flow. In (c) the disturbance is viewed normal to its axis. The picture is taken with flow in the tunnel. It is seen that the disturbance is cylindrical except for the inevitable end effects. In (d) the wake arising from the electrodes is shown. On the basis of such pictures it is concluded that the wake of the electrodes does not interfere with the disturbance or with the flow over a pitot tube used in the tunnel.

Figure 19 shows the speeds of flow deduced from the measurements of d and Δt. Each point refers to a different run and is taken at a different instant during the run. Points for the two arc-chamber

configurations mentioned before and referred to as "with facing electrodes" and "without facing electrodes" are included (c.f. p.5). In taking data, Δt is varied over the range 25 to 60 microseconds.

5.4 DISCUSSION

In drawing conclusions from Figure 19 it should be noted that points below 8 milliseconds are taken during the transient state of flow in the tunnel, while points at 8 milliseconds and above apply to the quasi-steady flow.

It is apparent from Figure 19 that the points belonging to each of the arc-chamber configurations fall into a distinct group. As mentioned before, all the runs are made at the same nominal initial conditions in the arc chamber. In view of the inevitable differences that exist in the actual initial conditions for the different runs and in the arc-chamber conditions corresponding to the different instants when the measurements are made, it is not intended to go into a discussion of the agreement or lack of it between the points corresponding to each specific configuration. We shall concern ourselves only with the difference exhibited by the two groups and inquire into the nature of the consequences that follow from such a difference. An obvious conclusion is, of course, that the speed of flow is strongly dependent on the arc-chamber configuration.

In this connection it may be recalled that Lukasiewicz et al. (1960) reported similar dependence on arc-chamber configuration of the results of measurements in a hotshot tunnel of drag of bodies and of stagnation-point heat-transfer rates. The differences in the measured data for different arc-chamber configurations and the disagreement between the measured and theoretical results have been attributed to the effects of contamination in the test-section stream arising out of the processes in the arc chamber. Efforts have been made to estimate these effects and considerable effort has been invested, notably by the Tullahoma group [see, for instance, van der Bliek et al. (1961)], in achieving a suitable arc-chamber design that would result in as low a level of contamination as possible. It is found that even with considerable reduction in the contamination level, the measured stagnation-point heat-transfer rates are still not satisfactory. Within this background, let us look into the nature of the consequences that follow from the difference exhibited by the measured speeds of flow for the arc-chamber types under investigation.

In Figure 20 we show the ratio of the calculated speed of flow, denoted by V_c, to the measured speed of flow, denoted by V. The speed V_c is calculated as mentioned before (see section 3.0) following the method given by Grabau et al. (1961). In Figure 20, points corresponding to the transient state of the flow in the tunnel are not shown. Again, we observe that the points belonging to each arc-chamber configuration form a distinct group. Further, the ratio V_c/V for each group is generally different from unity, the value one would normally

expect. This means that the calculated speed is not only not equal to the measured or actual speed of flow but is different for the two types of arc chamber even for the same nominal initial conditions.

The implications of this situation are significant.* The speed of flow V and the stagnation enthalpy h_o of the stream are related according to the equation

$$h_o = \frac{1}{2n} V^2 \tag{1}$$

where

$$n = 1 - \frac{h}{h_o}$$

h being the local enthalpy in the stream. Under the existing flow conditions, the quantity n is nearly equal to unity and is essentially a constant. Let us denote by $(h_o)_m$ the stagnation enthalpy corresponding to the measured speed of flow V. We shall refer to this enthalpy as the actual stagnation enthalpy. Let $(h_o)_c$ denote the stagnation enthalpy computed on the basis of the measured arc-chamber pressure p_o and the assumption of uniform thermodynamic state of the gas at every instant in the arc chamber. We shall refer to this as the computed (or calculated) stagnation enthalpy in the arc chamber, or simply as the computed (or calculated) stagnation enthalpy. This, of course, corresponds to the calculated speed V_c. Extending the foregoing notation throughout the following discussion we shall use the subscript c to denote any quantity obtained by calculation, according to the relations given by Grabau et al. (1961), from the pressure p_o measured in the arc chamber and the pitot pressure p_s measured in the test section. Similarly, we shall use the subscript m to denote any quantity obtained by calculation, according to the same relations, but from the speed of flow V and the measured pitot pressure p_s. With this notation, using Eq. (1), we obtain

$$\frac{(h_o)_c}{(h_o)_m} = \frac{V_c^2}{V^2} \cdot \frac{n_m}{n_c}$$

It is reasonable to assume, as mentioned above, that the quantity n remains essentially a constant. It follows therefore that

$$\frac{(h_o)_c}{(h_o)_m} = \frac{V_c^2}{V^2} \tag{2}$$

The ratio $(h_o)_c/(h_o)_m$ corresponding to the present measured values of the speed of flow is shown in Figure 21. For the "with

*The reader not interested in the following details may turn to page 22 where the main results are summarized.

facing electrodes" configuration, the computed stagnation enthalpy is about 98 to 140 percent of the actual value, while for the "without facing electrodes" configuration it ranges from 67 to 86 percent of the actual value. Thus, the stagnation enthalpy in the arc chamber as presently calculated on the basis of measured arc-chamber pressure and the assumption of uniform thermodynamic conditions at every instant, can differ considerably from the stagnation enthalpy that is actually found in the nozzle and test section. As we shall see, serious consequences result from this situation.

It is not clear what factors associated with the different configurations account for the foregoing enthalpy differences, and a consideration of them is outside the scope of the present investigation. Non-uniform heating of the gas in the chamber, with resulting non-uniformities in the thermodynamic quantities (notably enthalpy and density) may account for the situation. It is difficult to say, however, how these effects are brought about by the processes in the arc chamber and in what way they are dependent on the arc-chamber configuration.

Now, let us see what effect the discrepancy between the actual and computed stagnation enthalpy has on the various properties of the flow in the test section.* We first consider the density. The density ρ, the stagnation enthalpy h_o and the pitot pressure p_s in the test section are related by the equation

$$\rho = \frac{p_s}{h_o} \frac{1}{n[2 - r(1 - w)]} \tag{3}$$

where r is the ratio of the density ahead to the density behind a normal shock in the test section and w is equal to $M_2^2/4$, M_2 being the Mach number behind the normal shock. The density ratio is less than 0.15 and for the present flow conditions the quantity (1-w) is very nearly equal to unity. An average value of 0.97 will be assumed for this quantity. On the basis of Eq. (3), the ratio of the test-section densities corresponding respectively to the calculated and actual stagnation enthalpies is given by

$$\frac{\rho_c}{\rho_m} = \frac{(h_o)_m}{(h_o)_c} \frac{n_m}{n_c} \left[\frac{2 - r_m(1 - w)}{2 - r_c(1 - w)}\right]$$

Recall that the pitot pressure p_s is a measured quantity, the same value of which is used in calculating both ρ_c and ρ_m. We assume, as before, that n_c/n_m is equal to one. For the present flow conditions r may vary at most from 0.1 to 0.15. Correspondingly the

*For the derivation of the relations, used in the following, between the various flow quantities, reference may be made to Graubau et al. (1961).

quantity in the square brackets of the above relation may vary from 0.98 to 1.02. Assuming that it is unity, we may thus write with good accuracy

$$\frac{\rho_c}{\rho_m} = \frac{(h_o)_m}{(h_o)_c} \tag{4}$$

Consider next the static pressure p in the test section. The static pressure and the pitot pressure in the test section are related by

$$p = p_s - q[2 - r(1 - w)] \tag{5}$$

where q is the dynamic pressure $(1/2)\rho V^2$ in the test section. It follows, therefore, that

$$\frac{p_c}{p_m} = \frac{p_s - q_c[2 - r_c(1 - w)]}{p_s - q_m[2 - r_m(1 - w)]} \tag{6}$$

On the basis of the equations (2) and (4), we see that the values of the dynamic pressure corresponding to the calculated and actual stagnation enthalpies are equal, for we have

$$\frac{q_c}{q_m} = \frac{\rho_c}{\rho_m}\frac{V_c^2}{V^2} = \frac{(h_o)_m}{(h_o)_c}\frac{(h_o)_c}{(h_o)_m} = 1 \tag{7}$$

We may, therefore, rewrite equation (6) as

$$\frac{p_c}{p_m} = \frac{p_s - q[2 - r_c(1 - w)]}{p_s - q[2 - r_m(1 - w)]} \tag{8}$$

with the notation

$$q = q_c = q_m$$

We thus see that the difference between p_c and p_m is due to the difference between the factors $[2 - r_c(1 - w)]$ and $[2 - r_m(1 - w)]$. The factor $[2 - r(1 - w)]$ may vary at most from 1.854 to 1.903 corresponding to the maximum possible variation of 0.1 to 0.15 in r. Disregarding the variation in the factor $[2 - r(1 - w)]$ we may say that approximately

$$\frac{p_c}{p_m} \simeq 1 \tag{9}$$

The gas in the test section is essentially a perfect gas with constant specific heats. For conditions in the test section we may therefore write that

$$\frac{h}{RT} = \frac{h\rho}{p} = \text{constant} \tag{10}$$

where T denotes the temperature of the test-section stream. From relations (4), (9), and (10) we see that the ratio of the test-section temperatures corresponding to the calculated and actual stagnation enthalpies is given by

$$\frac{T_c}{T_m} = \frac{p_c}{p_m} \cdot \frac{\rho_m}{\rho_c} = \frac{(h_o)_c}{(h_o)_m} \tag{11}$$

The speed of sound in the test section is proportional to the square root of the temperature. Therefore, we obtain that

$$\frac{a_c}{a_m} = \sqrt{\frac{T_c}{T_m}} = \sqrt{\frac{(h_o)_c}{(h_o)_m}} \tag{12}$$

On the basis of relations (2) and (12), it follows that the Mach numbers in the test section corresponding to the calculated and actual stagnation enthalpies are equal, that is

$$\frac{M_c}{M_m} = \frac{V_c}{V} \frac{a_m}{a_c} = 1 \tag{13}$$

The viscosity μ of the gas in the test section is related to the temperature T as follows (where T is in ^{o}K and μ in lb/ft-sec)

$$\mu = 0.924 \times 10^{-6} \frac{T^{3/2}}{T + 100}$$

Therefore, we have

$$\frac{\mu_c}{\mu_m} = \left(\frac{T_c}{T_m}\right)^{3/2} \frac{T_m + 100}{T_c + 100}$$

$$= \left[\frac{(h_o)_c}{(h_o)_m}\right]^{3/2} \frac{T_m + 100}{T_c + 100} \tag{14}$$

The Reynolds numbers in the test section corresponding to the calculated and actual stagnation enthalpies are therefore related by

$$\frac{(Re)_c}{(Re)_m} = \frac{\rho_c}{\rho_m}\frac{V_c}{V}\frac{\mu_m}{\mu_c} = \left[\frac{(h_o)_m}{(h_o)_c}\right]^2 \frac{T_c + 100}{T_m + 100} \tag{15}$$

in view of Eqs. (2), (4) and (14).

We thus see that the Reynolds number, static temperature and density are affected by the discrepancy between the calculated and actual stagnation enthalpies, while the Mach number and the static pressure remain practically unaffected. The dynamic pressure is unaffected. This means that non-dimensional coefficients such as pressure and force coefficients formed from measured pressures and forces on a body and the computed dynamic pressure q_c will not be in error. One cannot assert, however, that those coefficients correspond to the calculated free-stream conditions.

Next consider the effect on conditions immediately behind a shock wave on the stagnation steamline of a pitot probe or model, i.e., conditions immediately behind a normal shock in the test section. We shall denote these by the first subscript 2.

The density ρ_2 behind the shock is given by

$$\rho_2 = \frac{\rho}{r} \tag{16}$$

where r is the density ratio ρ/ρ_2 to be computed from the relation

$$r = \frac{1}{2n\left(\frac{h_o \rho_s}{p_s}\right) - 1} \tag{17}$$

In this relation h_o and p_s are considered known, when ρ_s is also known from the equation of state. The ratio of the values of the density ρ_2 corresponding to the computed and actual stagnation enthalpies is then

$$\frac{(\rho_2)_c}{(\rho_2)_m} = \frac{r_m}{r_c}\left(\frac{\rho_c}{\rho_m}\right) = \left(\frac{r_m}{r_c}\right)\left(\frac{(h_o)_m}{(h_o)_c}\right) \tag{18}$$

using relation (4). The ratio r_c/r_m is given by

$$\frac{r_c}{r_m} = \frac{2\, n_m \dfrac{(h_o)_m (\rho_s)_m}{p_s} - 1}{2\, n_c \dfrac{(h_o)_c (\rho_s)_c}{p_s} - 1}$$

In the range of the present flow conditions, $h_o\rho_s/p_s$ can be expressed in terms of h_o and p_s by means of an equation. It is, however, not possible to write r_c/r_m explicitly in terms of $(h_o)_c/(h_o)_m$. Therefore, to carry on with the discussion we shall retain r_c/r_m as it stands and bear in mind that it may be different from unity. Corresponding to the maximum variation of 0.1 to 0.15 in r, the ratio r_c/r_m may lie in the range 0.67 to 1.5.

The static pressure p_2 immediately behind the shock is given by

$$p_2 = 2p_s \frac{1 - r}{2 - r(1 - w)} \tag{19}$$

Therefore, the values of p_2 corresponding to the calculated and actual stagnation enthalpies are related by

$$\frac{(p_2)_c}{(p_2)_m} = \frac{1 - r_c}{1 - r_m} \left[\frac{2 - r_m(1 - w)}{2 - r_c(1 - w)}\right] \tag{20}$$

It is reasonable to assume, as before, that the quantity in the square brackets is equal to unity. Hence, relation (20) may be written as

$$\frac{(p_2)_c}{(p_2)_m} = \frac{1 - r_c}{1 - r_m} \tag{21}$$

The temperature T_2 immediately behind the shock is related to p_2 and ρ_2 according to the equation of state

$$T_2 = \frac{1}{RZ_2} \frac{p_2}{\rho_2} \tag{22}$$

where Z_2 is the compressibility factor behind the shock. From Eqs. (22), (21) and (18), it follows that

$$\frac{(T_2)_c}{(T_2)_m} = \frac{(Z_2)_m}{(Z_2)_c} \left(\frac{1 - r_c}{1 - r_m}\right) \left(\frac{r_c}{r_m}\right) \frac{(h_o)_c}{(h_o)_m} \tag{23}$$

The compressibility factor Z_2 is a function of h_2 and p_2 and, therefore, $(Z_2)_c$ need not be equal to $(Z_2)_m$. However, in the range of the flow conditions we are considering, the maximum variation of Z_2 is approximately 1.02 to 1.00. Hence in Eq. (23) we may assume that $(Z_2)_m/(Z_2)_c$ is equal to unity. Further, since the density ratio r, being less than 0.15, is small compared to one, we can set

$$\left(\frac{1 - r_c}{1 - r_m}\right) \left(\frac{r_c}{r_m}\right) \simeq \frac{r_c}{r_m}$$

With these approximations relation (23) may be rewritten as

$$\frac{(T_2)_c}{(T_2)_m} = \left(\frac{r_c}{r_m}\right) \frac{(h_o)_c}{(h_o)_m} \tag{24}$$

Now, we consider the effect of the discrepancy between the calculated and actual stagnation enthalpies on the stagnation density ρ_s and stagnation temperature T_s behind the shock. For the present range of flow conditions, the numerical value of the function $h\rho/p$ changes very little from the back of the shock to the stagnation point. Thus, we have to a good approximation

$$\frac{h_o \rho_s}{p_s} = \frac{h_2 \rho_2}{p_2} \tag{25}$$

Since h_2 can be expressed as

$$h_2 = (1 - nr^2)h_o$$

equation (22) can be written in the form

$$\frac{\rho_s}{p_s} = (1 - nr^2) \frac{\rho_2}{p_2} \tag{26}$$

Using relations (26), (21), and (18) we then obtain

$$\frac{(\rho_s)_c}{(\rho_s)_m} = \left(\frac{1 - n_c r_c^2}{1 - r_c}\right)\left(\frac{1 - r_m}{1 - n_m r_m^2}\right) \frac{r_m}{r_c} \frac{(h_o)_m}{(h_o)_c} \tag{27}$$

In this expression, again, since $r \ll 1$, we can make the following approximations:

$$\frac{1 - n_c r_c^2}{1 - r_c} = 1 + r_c$$

$$\frac{1 - n_m r_m^2}{1 - r_m} = 1 + r_m$$

and

$$\frac{1 - n_c r_c^2}{1 - r_c} \quad \frac{1 - r_m}{1 - n_m r_m^2} \left(\frac{r_m}{r_c}\right) \simeq \frac{1 + r_c}{1 + r_m} \quad \frac{r_m}{r_c} \quad \simeq \frac{r_m}{r_c}$$

Then relation (27) may be written to a good approximation as

$$\frac{(\rho_s)_c}{(\rho_s)_m} = \left(\frac{r_m}{r_c}\right) \frac{(h_o)_m}{(h_o)_c} \tag{28}$$

The stagnation temperature T_s behind the shock is related to p_s and ρ_s by the equation of state

$$T_s = \frac{1}{RZ_s} \frac{p_s}{\rho_s} \tag{29}$$

where Z_s is the compressibility factor associated with the stagnation conditions p_s and ρ_s. From Eq. (29) we obtain

$$\frac{(T_s)_c}{(T_s)_m} = \frac{(Z_s)_m}{(Z_s)_c} \frac{(\rho_s)_m}{(\rho_s)_c} \tag{30}$$

The compressibility factor Z_s changes very little for the present flow conditions. Hence, setting $(Z_s)_m/(Z_s)_c$ equal to one and using equation (28), relation (30) may be written to good approximation as

$$\frac{(T_s)_c}{(T_s)_m} = \frac{(\rho_s)_m}{(\rho_s)_c} = \left(\frac{r_c}{r_m}\right) \frac{(h_o)_c}{(h_o)_m} \tag{31}$$

The viscosity of the gas behind the shock is very nearly a linear function of temperature. However, for simplicity, we shall assume that the viscosity behind the shock is proportional to the temperature. (No serious error is introduced by this assumption). Therefore, using relations (24) and (31) we have

$$\frac{(\mu_s)_c}{(\mu_s)_m} = \frac{(T_2)_c}{(T_2)_m} \simeq \left(\frac{r_c}{r_m}\right) \frac{(h_o)_c}{(h_o)_m} \tag{32}$$

and

$$\frac{(\mu_s)_c}{(\mu_s)_m} = \frac{(T_s)_c}{(T_s)_m} \simeq \left(\frac{r_c}{r_m}\right) \frac{(h_o)_c}{(h_o)_m} \tag{33}$$

The Reynolds number behind the shock is affected as follows:

$$\frac{(Re_2)_c}{(Re_2)_m} = \frac{(\rho_2)_c}{(\rho_2)_c} \frac{(V_2)_c}{(V_2)_m} \frac{(\mu_2)_m}{(\mu_2)_c}$$

$$= \frac{\rho_c}{\rho_m} \frac{V_c}{V} \frac{(\mu_2)_m}{(\mu_2)_c}$$

(continued)

(continuation)

$$\frac{(Re_2)_c}{(Re_2)_m} \simeq \left(\frac{r_m}{r_c}\right)\left[\frac{(h_o)_m}{(h_o)_c}\right]^{3/2} \tag{34}$$

We thus see that the discrepancy between the computed and actual stagnation enthalpies affects the values of all the flow quantities behind the shock.

Now let us look into the stagnation-point heat-transfer rates evaluated on the basis of the Fay-Riddell (1958) theory. According to this theory, at the operating conditions under consideration the stagnation-point heat-transfer rate $\dot{q}_{th}$ is given by

$$\dot{q}_{th} = \text{const.}\ (\rho_s\mu_s)^{0.4}\, h_s \left(\frac{p_s}{\rho_s}\right)^{0.25} \tag{35}$$

where as before the subscript s denotes stagnation conditions behind the shock. (In writing this equation, it is assumed that $h_{wall}/h_s \ll 1$.) Note that $h_s = h_o$. Thus if $(\dot{q}_{th})_c$ denotes, as before, the value of $\dot{q}_{th}$ computed on the basis of the calculated stagnation enthalpy, and $(\dot{q}_{th})_m$ that on the basis of $(h_o)_m$, we have from relation (35)

$$\frac{(\dot{q}_{th})_c}{(\dot{q}_{th})_m} = \left[\frac{(\rho_s)_c(\mu_s)_c}{(\rho_s)_m(\mu_s)_m}\right]^{0.4} \frac{(h_o)_c}{(h_o)_m}\left[\frac{(\rho_s)_m}{(\rho_s)_c}\right]^{0.25} \tag{36}$$

From Eqs. (33) and (21), it follows that

$$\frac{(\rho_s)_c(\mu_s)_c}{(\rho_s)_m(\mu_s)_m} = 1$$

With this and relation (28), Eq. (36) becomes

$$\frac{(\dot{q}_{th})_c}{(\dot{q}_{th})_m} = \left(\frac{r_c}{r_m}\right)^{0.25} \cdot \left[\frac{(h_o)_c}{(h_o)_m}\right]^{1.25}$$

$$= \alpha \left[\frac{(h_o)_c}{(h_o)_m}\right]^{1.25} \tag{37}$$

where α is the quantity

$$\left(\frac{r_c}{r_m}\right)^{0.25}$$

For the present flow conditions, since the density ratio r may at most be in the range 0.1 to 0.15, the factor α will be in the range .904 to 1.107. Since in the present investigations $(h_o)_c/(h_o)_m$ varies from 0.67 to 1.40 (c.f. Fig. 21), the quantity

$$[(h_o)_c/(h_o)_m]^{1.25}$$

varies from 0.61 to 1.52. In view of these numbers, Eq. (37) shows that the theoretically evaluated stagnation-point heat-transfer rate can be in serious error if no account is taken of the possible discrepancy between the calculated and actual stagnation enthalpies. For instance, for the arc-chamber configurations under consideration, on the basis of Figure 21, we obtain the following information:

Configuration	Range of			
	$\frac{(h_o)_c}{(h_o)_m}$	$\frac{1}{\alpha}\frac{(\dot{q}_{th})_c}{(\dot{q}_{th})_m}$	$(\dot{q}_{th})_c/(\dot{q}_{th})_m$ for	
			$\alpha = .904$	$\alpha = 1.107$
with facing electrodes	0.98 - 1.40	0.98 - 1.52	0.88 - 1.37	1.08 - 1.68
without facing electrodes	0.67 - 0.86	0.61 - 0.83	0.55 - 0.75	0.68 - 0.92

Thus for the case "with facing electrodes" the theoretical heat-transfer rate calculated on the basis of the computed stagnation enthalpy $(h_o)_c$ is about 12 percent lower to 68 percent larger than the actual value calculated on the basis of the actual stagnation enthalpy $(h_o)_m$; for the case "without facing electrodes" it is about 8 to 45 percent lower than the actual value. Considerations of this nature might explain part of the large discrepancy observed in hotshot-type tunnels, between measured and theoretically evaluated stagnation-point heat-transfer rates. To resolve such a discrepancy, it is necessary, in light of the present discussion, to carry out for a given arc-chamber configuration simultaneous measurements of the speed of flow and the heat-transfer rate.

It is of interest to mention further that in applying theoretically evaluated corrections to measurements (when the evaluation involves the flow quantities) one should again bear in mind that the actual enthalpy $(h_o)_m$ may be different from the computed one $(h_o)_c$. For instance, consider the estimation given by Lukasiewicz et al. (1961) for the effect of particle impact (due to contamination) on heat-transfer measurements. According to their suggestion, the ratio of the particle-included heat-transfer rate $\dot{q}_p$ to the measured aerodynamic heat-transfer rate $\dot{q}_a$ at the stagnation point of a given body is

$$\frac{\dot{q}_p}{\dot{q}_a} \sim \left(\frac{\rho}{\sqrt{V}}\right)^{0.5} \sigma$$

where σ is the ratio of particle density to gas density. The calculations of Lukasiewicz et al. (1960) indicate that even a small amount of contamination, of the order of 2 or 3 percent, affects the stagnation-point heat-transfer rate by a factor of about 2 on typical models at the conditions of flow under discussion. If $(\dot{q}_p)_c$ denotes the heat-transfer rate estimated on the basis of $(h_o)_c$, i.e., on the basis of ρ_c and V_c, and $(\dot{q}_p)_m$ denotes that corresponding to the actual $(h_o)_m$, we obtain for fixed σ

$$\frac{(\dot{q}_p)_c}{(\dot{q}_p)_m} = \left(\frac{\rho_c}{\rho_m}\right)^{0.5} \left(\frac{V}{V_c}\right)^{0.25}$$

or, using relations (2) and (4),

$$\frac{(\dot{q}_p)_c}{(\dot{q}_p)_m} = \left[\frac{(h_o)_m}{(h_o)_c}\right]^{0.625} \tag{38}$$

This shows that whenever the computed and actual stagnation enthalpies are different, the theoretically evaluated correction to the measured heat-transfer rate will also be in error.

The preceding discussion may be summarized as follows:

The actual stagnation enthalpy may be different from the enthalpy calculated on the basis of the measured arc-chamber pressure $p_o(t)$ and the assumption of uniform thermodynamic conditions in the chamber. As a consequence of this difference, significant errors may occur in the values of the speed, density, temperature, and Reynolds number of the test-section stream calculated on the basis of the measured pressures $p_o(t)$ and $p_s(t)$. On the basis of the present considerations the static pressure, dynamic pressure, and Mach number are not in error. Discrepancies may occur between the calculated and actual values of after-shock conditions. As a result, theoretical estimates of quantities such as stagnation-point heat-transfer rates may be in considerable error. Similarly, theoretical estimates of corrections to measured values are likely to be in error.

On the basis of the above discussion one of the directions in which to proceed to achieve satisfactory untilization of the hotshot wind tunnel is clear. Since the thermodynamic state of the gas in the arc chamber cannot be known accurately on the basis of present practice, it is necessary to measure the time history of as many properties of the flow in the test section as possible. (For instance, time-resolved measurements of the speed of flow by schlieren or other

techniques may be made). The development of techniques for this purpose is therefore needed. The situation is particularly serious if one wishes to assess viscous effects in the flow through the tunnel or to extend the range of operation of the hotshot tunnel, when additional uncertainties will naturally arise.

5.5 SPEED OF SOUND AND DENSITY FROM SCHLIEREN MEASUREMENTS

We now take up briefly the question of determining directly by means of the schlieren measurements, the speed of sound and density in the stream. If the disturbance is acoustic, then, as pointed out before, the speed of sound is easily found. For practical reasons, the disturbance for the measurements reported here is not an acoustic wave. In such a case, the rate of growth of the disturbance front relative to the stream is no longer a constant. The rate of growth of the disturbance as a function of position and time depends on the energy put into the disturbance by the discharge, the initial (i.e., before the discharge) density and the ratio of the specific heats of the gas in the undisturbed stream. If the energy in the disturbance is sufficiently large and if it is assumed that the discharge occurs at a point or along a line, the rate of growth of the disturbance can be predicted closely by blast-wave theories; see for instance Sedov (1959). Using such theories, one can deduce from the measurements of the rate of growth of a blast wave in a stream, the density and/or speed of sound in the undisturbed stream. Instead of using the theory in conjunction with measurements, one may attempt to determine the density purely experimentally. This may be done in principle by comparing the rate of growth measured at varying test conditions but with the gas stationary. This possibility of deducing density was considered at Stanford. Exploratory tests had shown that several operational difficulties have to be overcome before determining the feasibility of the scheme. A main difficulty has been (with the present experimental set-up) in arranging the blast-wave conditions such that they are similar to those assumed in the theory. Further, the conditions of the blast-wave (such as the energy carried by the wave, the nature of the discharge of energy, etc.) with flow are likely to be different from those without flow. The seriousness of these differences has to be ascertained. It appears, at this stage, that a time-resolved measurement of the rate of growth of a disturbance relative to the actual stream might be a profitable approach to determine the feasibility of deducing the density and/or the speed of sound in the originally undisturbed stream.

6.0 STATE OF THE FLOW AS DEDUCED FROM SPEED-OF-FLOW AND PRESSURE MEASUREMENTS

If one measures the speed of flow $V(t)$ in the test section, the corresponding stagnation enthalpy $h_o(t)$ in the arc chamber can be derived to a good approximation from equation (1):

$$h_o = \frac{1}{2n} v^2$$

Then, if the arc-chamber pressure $p_o(t)$ is measured in addition, the effective thermodynamic state of the gas in the arc chamber as a function of time is completely determined. This procedure differs from that in current practice. Now, if one measures also the pitot pressure $p_s(t)$ in the test section and assumes one-dimensional adiabatic equilibrium flow through the nozzle, then all the flow quantities can be found. It should be appreciated that this sort of procedure is necessary if one wishes to investigate nonequilibrium effects in the nozzle flow when they occur.

Following the foregoing scheme, the state of the flow in the test section of the Stanford spark-heated tunnel has been found for those cases in which simultaneously measured values of flow speed and pitot pressure are available. As a matter of information, the results are given in the accompanying table. The table gives an idea of the range of values of the flow quantities under present operating conditions. Included in the table for comparison are measured wall pressures. The computed, effective area ratio at the test section is also given. For comparison the geometric area ratio at the location of the pitot tube is included.

SOME TYPICAL FLOW CONDITIONS IN THE STANFORD SPARK-HEATED TUNNEL

Nominal Initial Conditions: $T_o(t = 0) = 4000\ ^oK$

$p_o(t = 0) = 10{,}000$ psi

		Measured			Deduced						
Run Designation	Time sec	p_o psi	p_s psi	V ft/sec	ρ amagat	T ^oK	M	A_e/A^*	p psi	p_w psi	A_G/A^*
A	.008	7059	1.740	8456	.00154	65.3	15.7	7404	.00538	-	24200
B		6182	1.679	7681	.00179	52.7	15.8	6885	.00508	-	24200
C		6707	1.376	7475	.00155	46.5	16.4	8869	.00389	-	24200
D		6140	2.386	7369	.00277	56.3	14.7	4723	.00839	-	26000
E		5837	0.825	9700	.00055	64.4	18.1	12946	.00192	-	26000
F	.010	6060	0.755	10098	.00047	67.4	18.4	14622	.00162	-	26000
G		6050	1.355	9935	.00087	82.7	16.3	8110	.00385	-	26000
H		7788	1.308	7350	.00152	43.1	16.8	11556	.00362	-	27000
I	.012	5997	1.568	8020	.00154	57.6	15.8	6946	.00476	-	26000
J	.015	6074	0.949	9450	.00067	65.1	17.5	11618	.00235	.00298	27000
K		6242	0.917	7490	.00103	40.6	17.6	12400	.00226	.00230	27000
L	.020	5262	0.658	8670	.00055	49.2	18.5	14499	.00146	.00357	27000
M		5356	0.692	7150	.00085	34.2	18.3	14133	.00156	.00309	27000
N		7380	0.839	6540	.00124	29.9	17.9	16083	.00199	.00201	27000
O	.024	5116	0.785	7650	.00085	41.9	17.7	11830	.00191	-	27000
P	.025	5150	0.897	8900	.00074	59.4	17.3	10365	.00236	.00232	27000
Q	.030	4516	0.515	8380	.00046	43.0	19.1	16110	.00107	.00150	27000
R		3749	0.493	7310	.00058	33.3	18.4	13426	.00145	.00234	27000
S	.035	3639	0.624	8560	.00054	49.7	18.0	10708	.00146	.00262	27000
T		3760	0.578	6890	.00077	31.6	18.2	11950	.00131	.00168	27000

p_w is the test-section wall pressure measured at x = 113.5" (pitot probe at x = 117")

REFERENCES

Cox, R. N., 1959, Recent Hyperballistics Research at A.R.D.E. Hypersonic Flow, Proceedings of the Eleventh Symposium of the Colston Research Society.

Cunningham, B. E., and Kraus, S., 1958, Experimental Investigation of the Effect of Yaw on Rates of Heat Transfer to Transverse Circular Cylinders in a 6500-Foot-Per-Second Hypersonic Air Stream, National Advisory Committee for Aeronautics, NACA RM A58E19.

Earheart, Jr., W. T., and Bynum, D.S., 1960, Hypervelocity Arc-Tunnel Instrumentation. Inst. of the Aero. Sci., Proceedings of the Hypervelocity Techniques Symposium 1960.

Elliott, D. E., 1955, The Measurement of High Speed Air Velocity and Temperature in Dissociated Air , Journal of the Aeronautical Sciences, vol. 25, p. 73.

Emanuel, G., and Vincenti, W. G., 1962, Method for Calculation of the One-Dimensional Nonequilibrium Flow of a General Gas Mixture Through a Hypersonic Nozzle, Arnold Engineering Development Center, AEDC TDR-62-131.

Fay, J. A., and Riddell, F. R., 1958, Theory of Stagnation Point Heat Transfer in Dissociated Air, Journal of the Aeronautical Sciences, vol. 25, p. 73.

Grabau, M., Humphrey, R. L., and Little, W. J., 1961, Determination of Test-Section After-Shock and Stagnation Conditions in Hotshot Tunnels using Real Nitrogen at Temperatures from 3000 to 4000°K, Arnold Engineering Development Center, AEDC TN-61-82.

Holder, D. W., and North, R. J., 1956, Schlieren Methods, Part 1 of Optical Methods for Examining the Flow in High-Speed Wind Tunnels, AGARD, AGARDograph 23.

Karamcheti, K., Vali, W., Kyser, B. J., 1962, Optical Techniques for the Measurement of Velocity, Density, Temperature, and Contamination Level in a Spark Heated Hypervelocity Wind Tunnel, Proceedings of the Second Symposium on Hypervelocity Techniques, Denver Research Institute, Distributed by Plenum Press.

Lukasiewicz, J., Harris, W. G., Jackson, R., van der Bliek, J. A., and Miller, R. M., 1960, Development of Capacitance and Inductance Driven Hotshot Tunnels, Institute of the Aeronautical Sciences, Proceedings of the Hypervelocity Techniques Symposium 1960.

Merritt, G. E., 1961, Velocity Measurements in the University of Southampton Hypersonic Gun Tunnel, University of Southampton, AASU Report No. 172.

Mulkey, M. R., Earheart, Jr., W. T., and McAdams, Jr., E. E., 1958, Pressure Measurements in an Arc-Discharge Wind Tunnel, Arnold Engineering Development Center, AEDC-TN-58-16.

Sedov, L. I., 1959, Similarity and Dimensional Methods in Mechanics, Academic Press.

Thomas, G. M., 1961, A Schlieren System for the Spark-Heated Hypersonic Wind Tunnel and Studies of Blast Wave Propagation, Stanford University Department of Aeronautical Engineering, Engineering Thesis.

Vali, W., and deVoto, R., 1962, A Two-Color Pyrometer for the Measurement of Temperature and Contamination Level in a Spark-Heated Hypervelocity Wind Tunnel, Arnold Engineering Development Center, AEDC TDR-62-174.

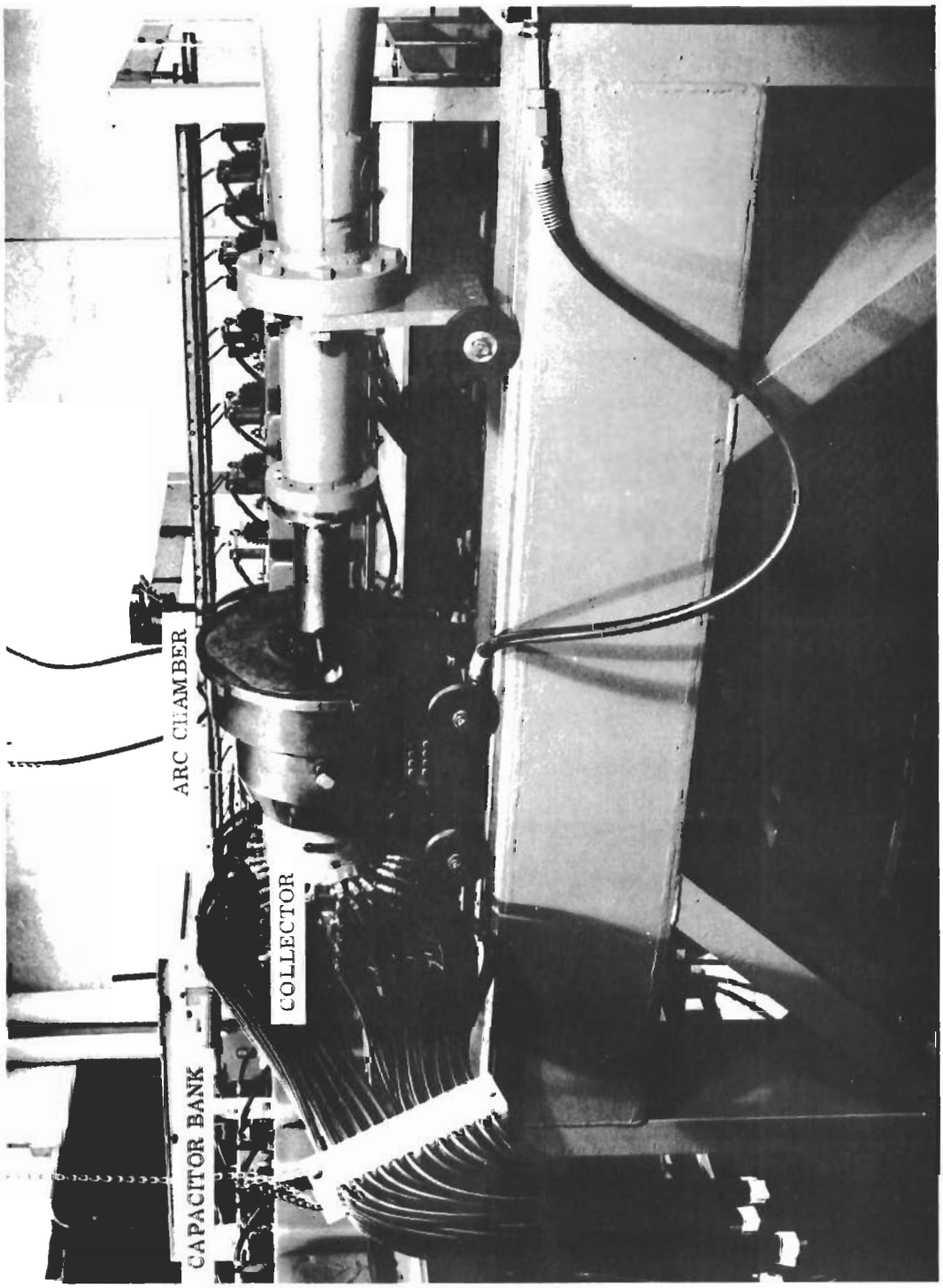

Fig. 1 Capacitor Bank and Arc Chamber

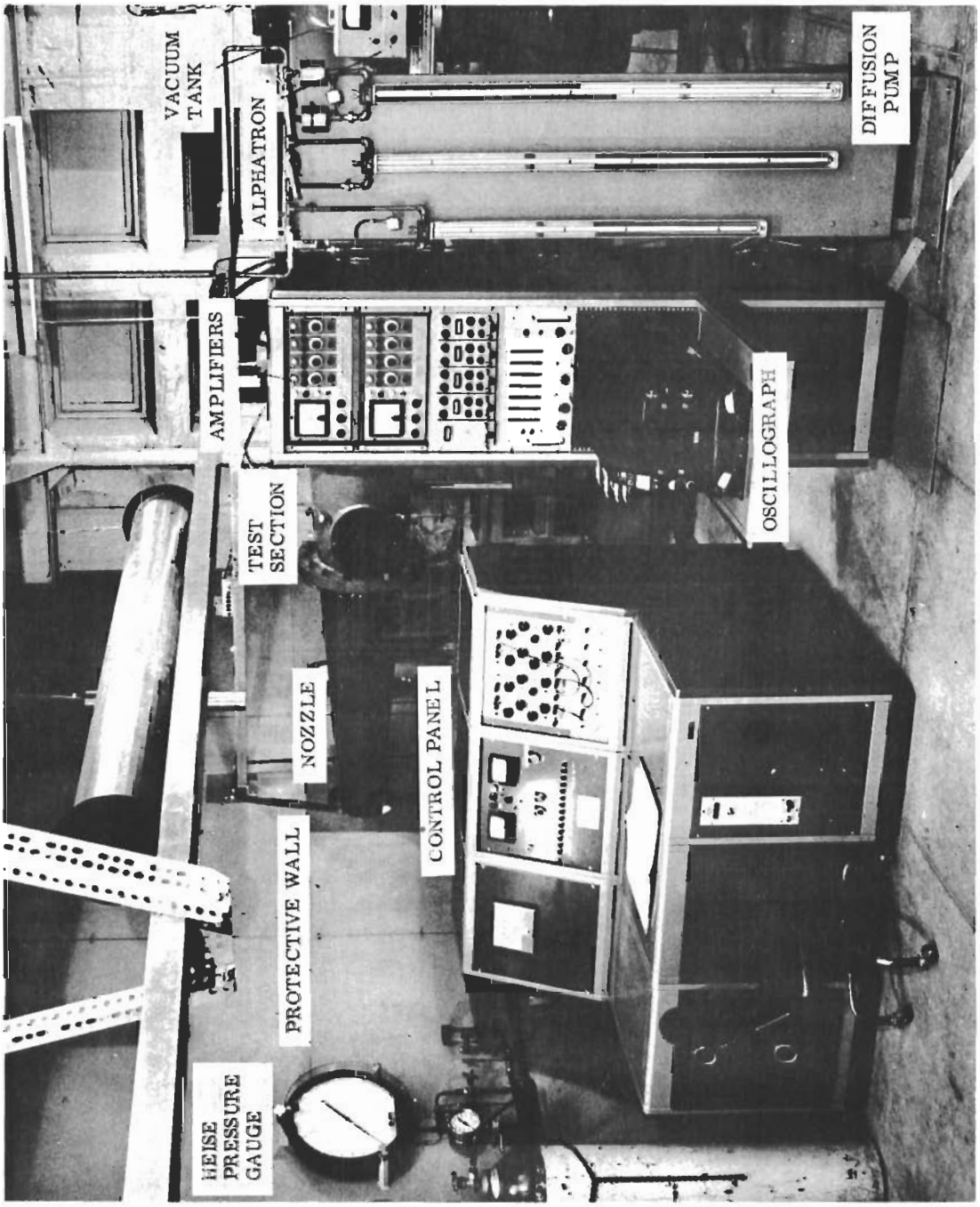

Fig. 2 Tunnel and Associated Equipment

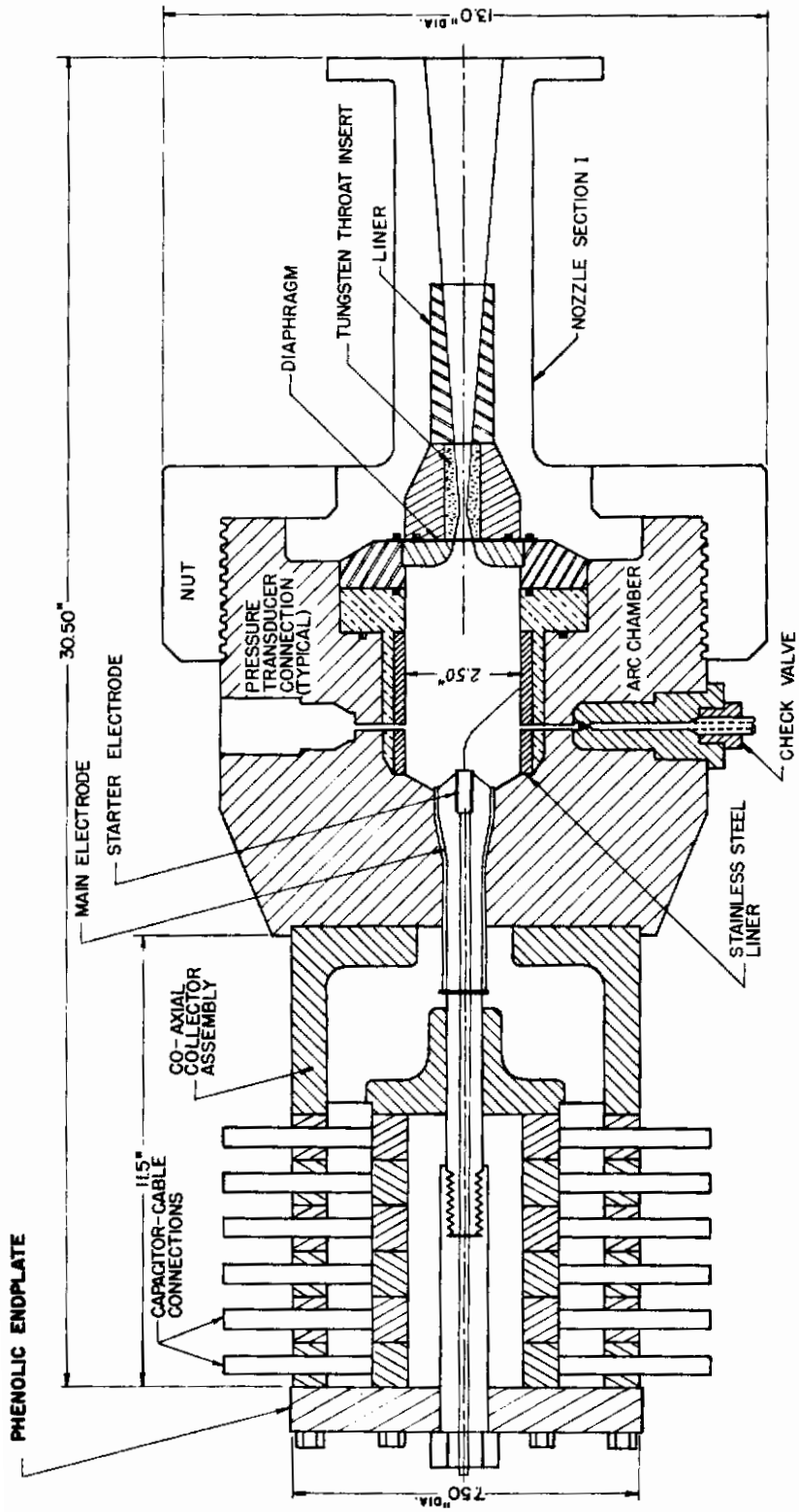

Fig. 3 Arc Chamber & Collector Assembly

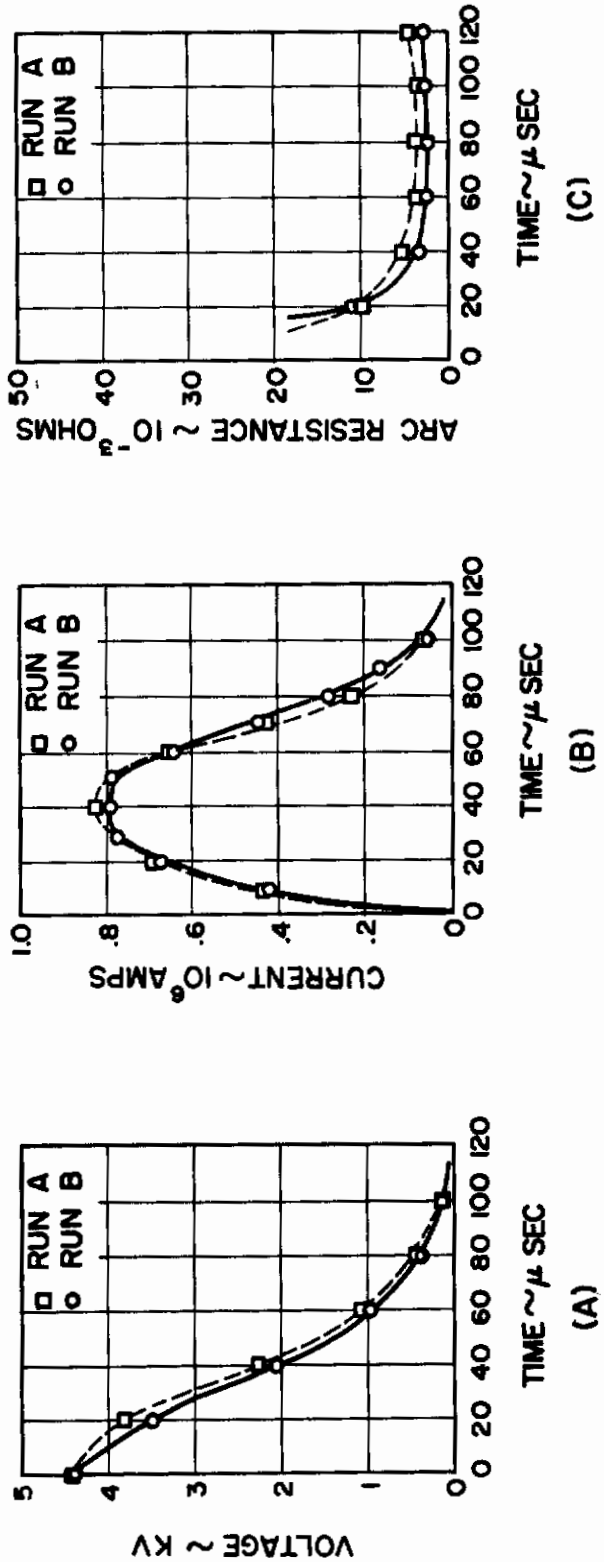

Fig. 4 Energy Discharge Characteristics

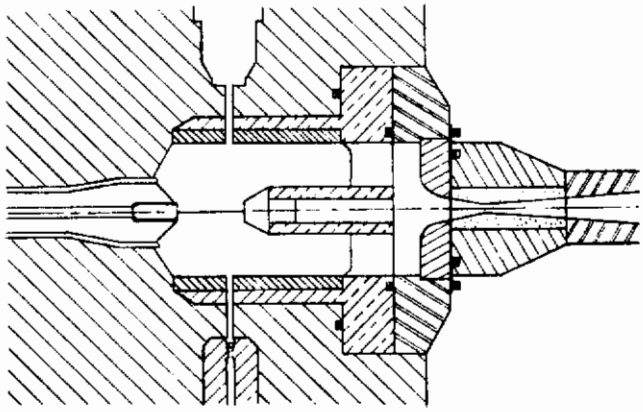

a. Arc Chamber with Facing Electrodes

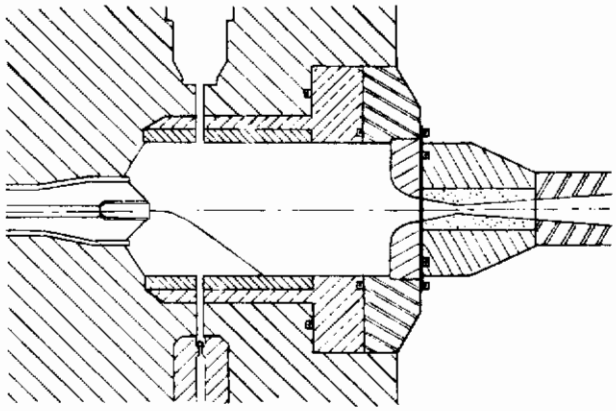

b. Arc Chamber without Facing Electrons

Fig. 5

NOTES:
NOZZLE: TOTAL INCLUDED ANGLE 8°20'.
LENGTH 110".
TEST SECTION LENGTH 24".

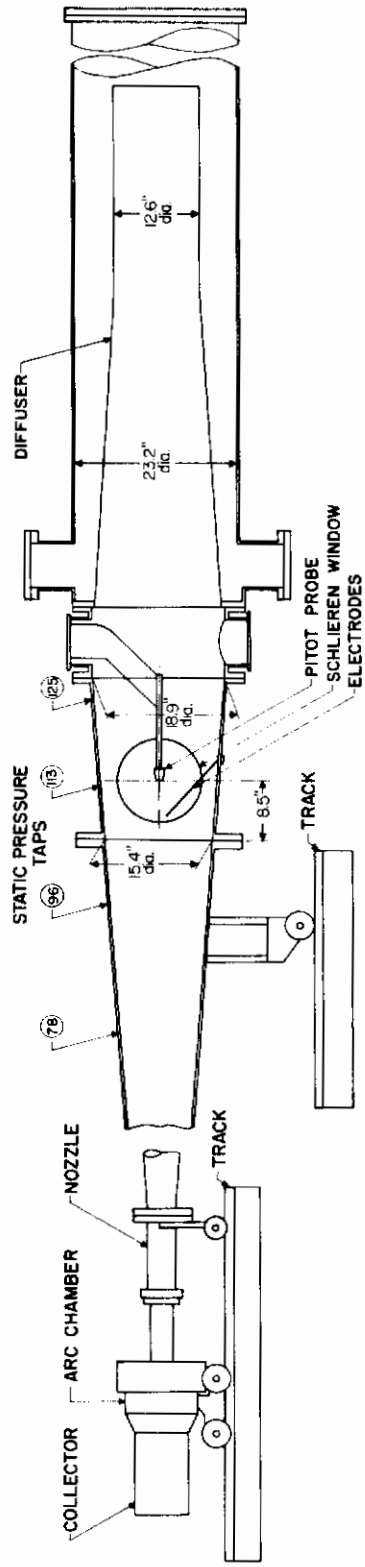

Fig. 6 Main Features of Nozzle, Test Section and Diffuser

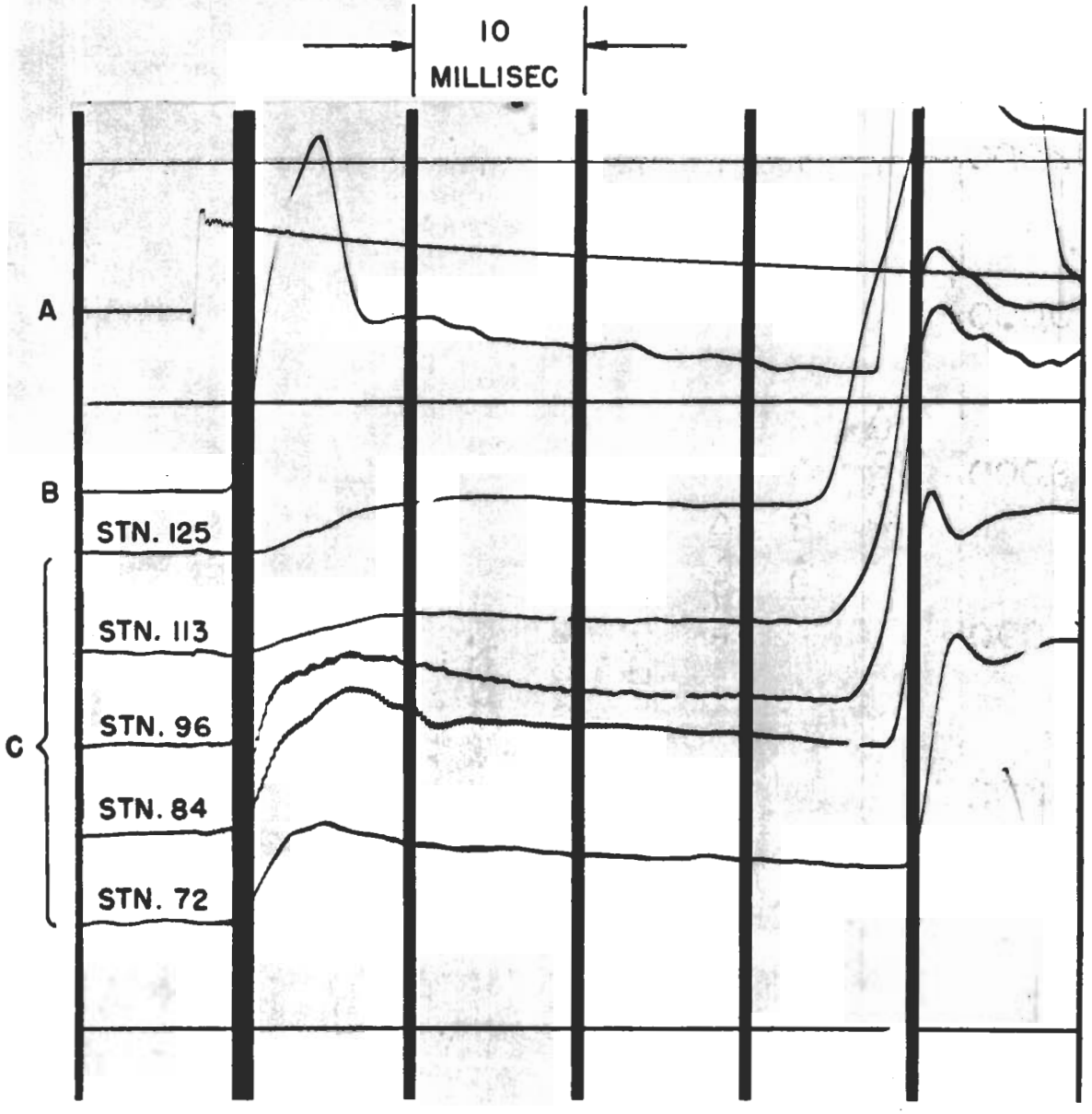

A. Arc-Chamber Pressure
B. Pitot Pressure at Station 113
C. Static Pressures on Tunnel Wall

Fig. 7 Typical Pressure Traces

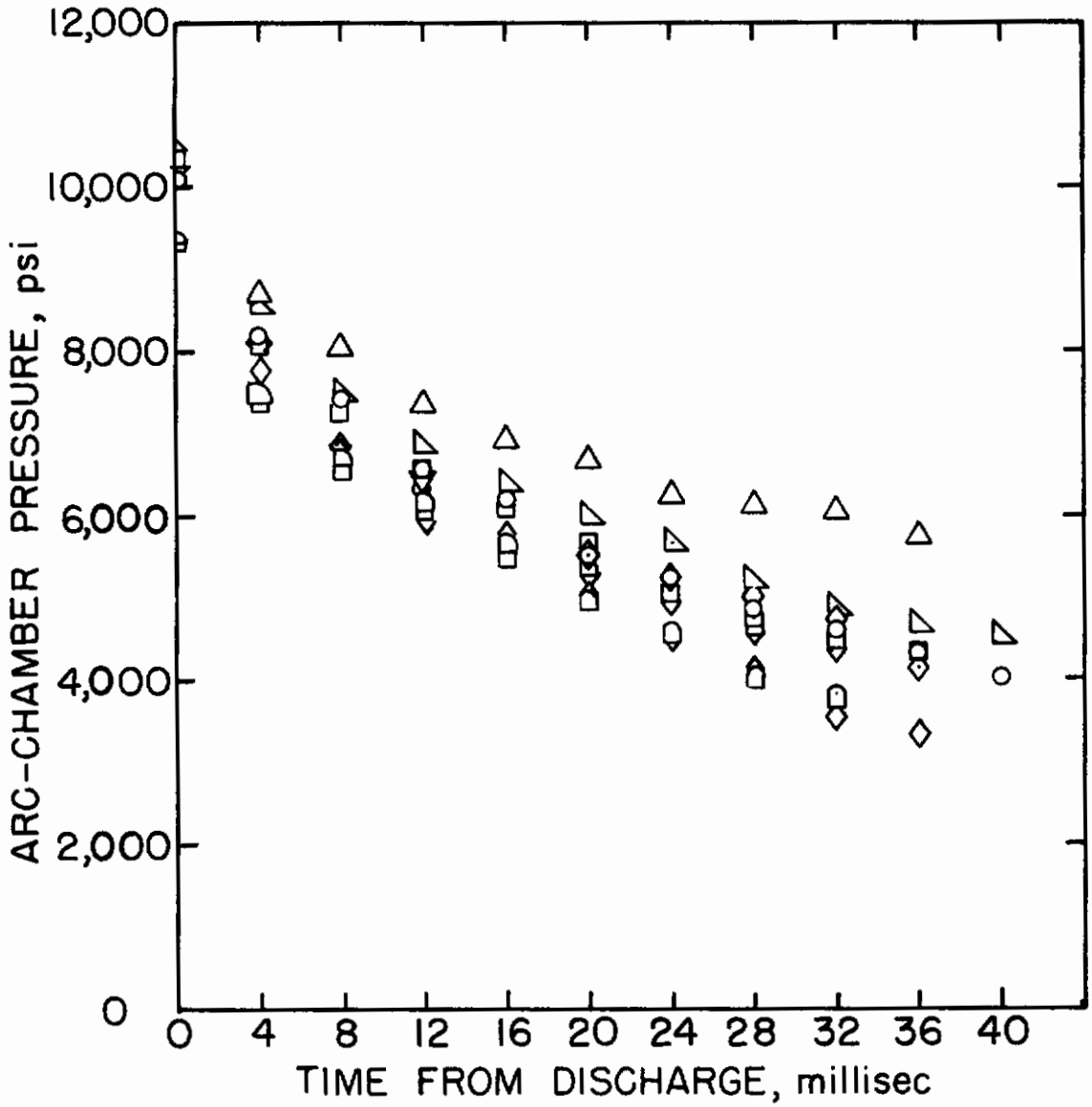

Fig. 8 Arc-Chamber Pressure as a Function of Time

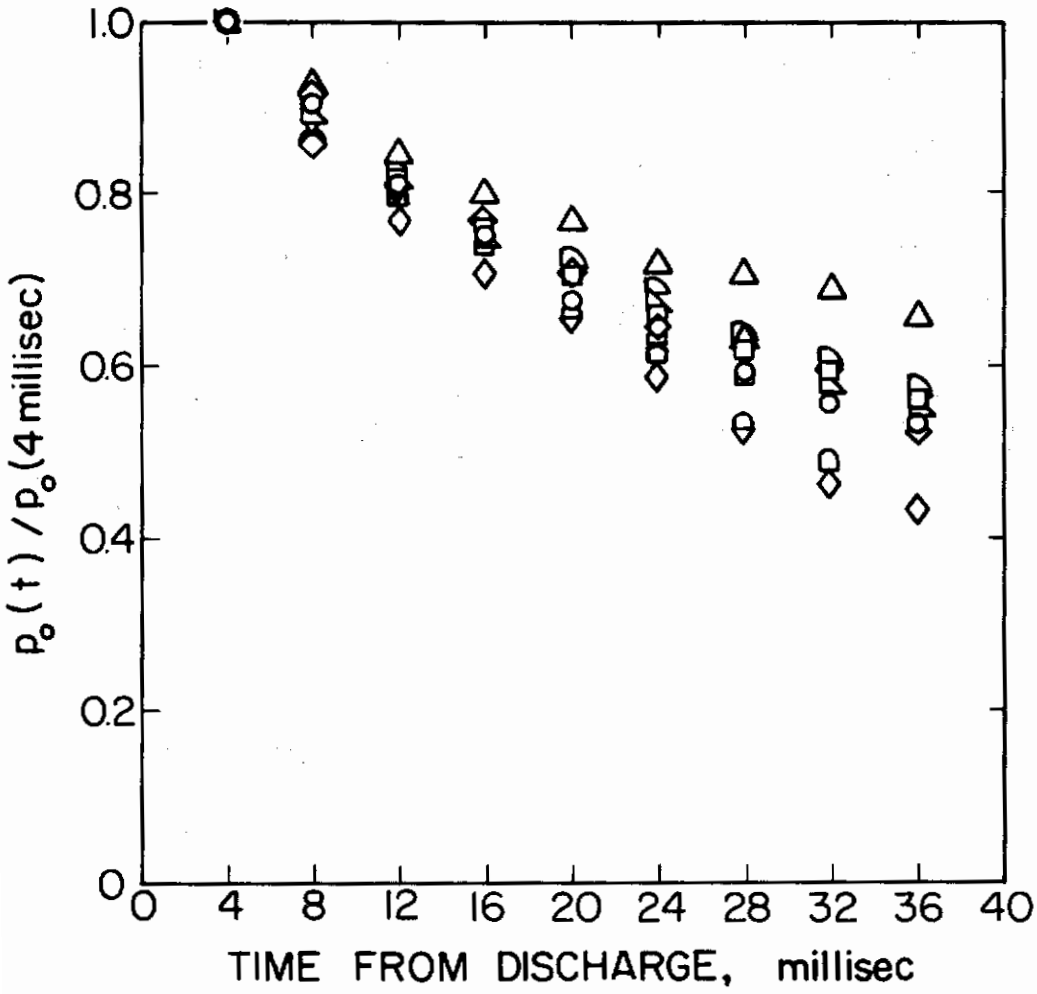

Fig. 9 Arc-Chamber Pressure Decay

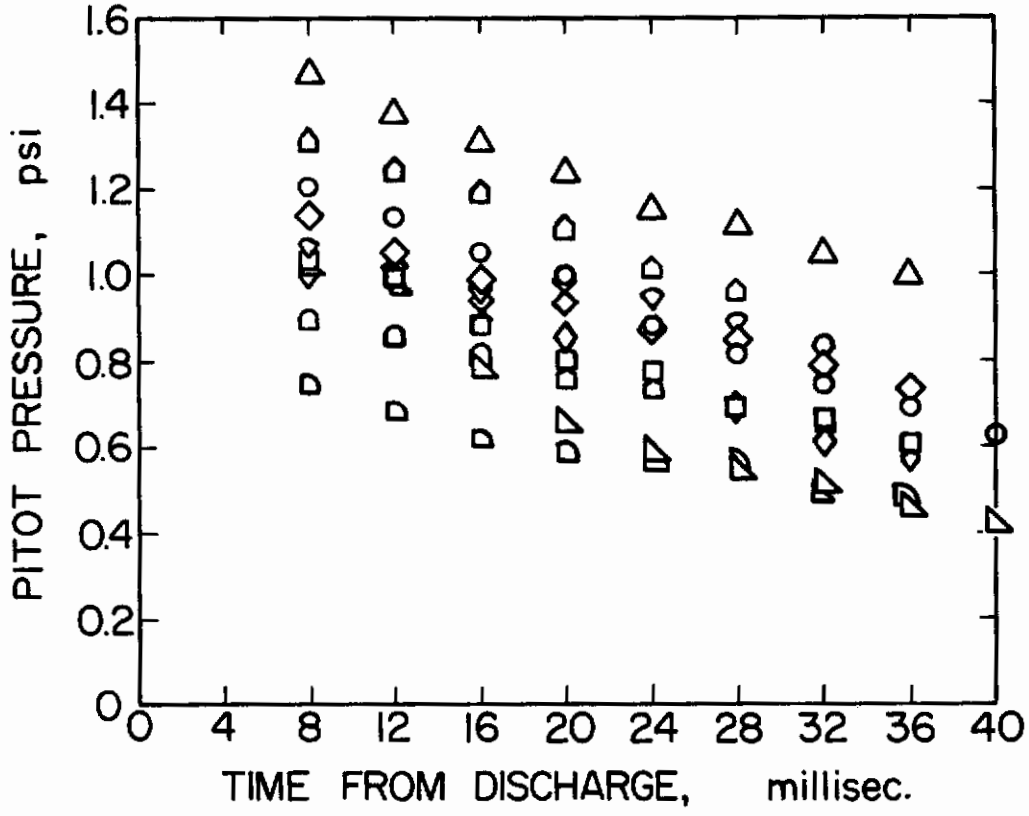

Fig. 10 Pitot Probe Pressure

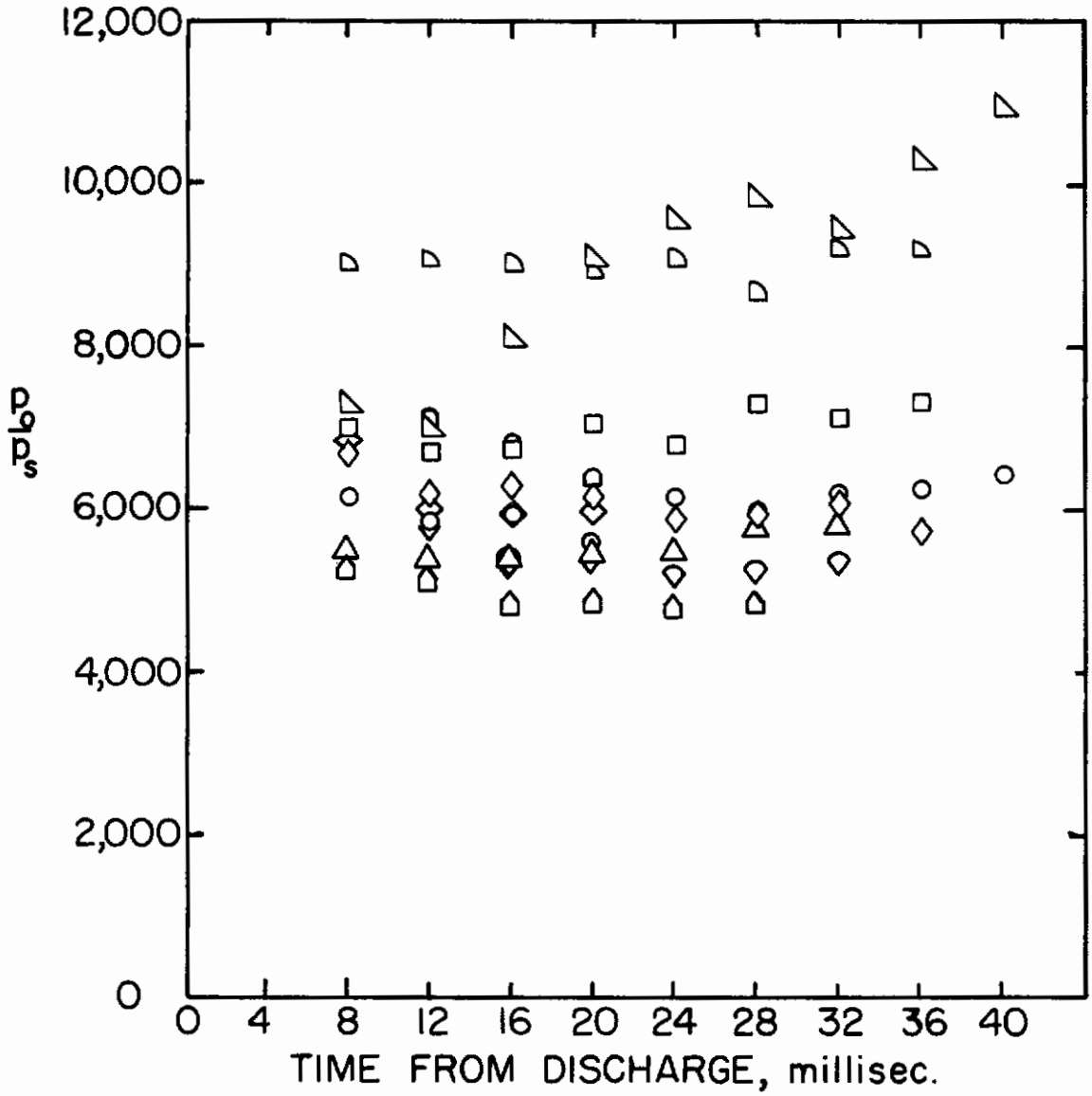

Fig. 11 Ratio of Arc-Chamber Pressure to Pitot Pressure

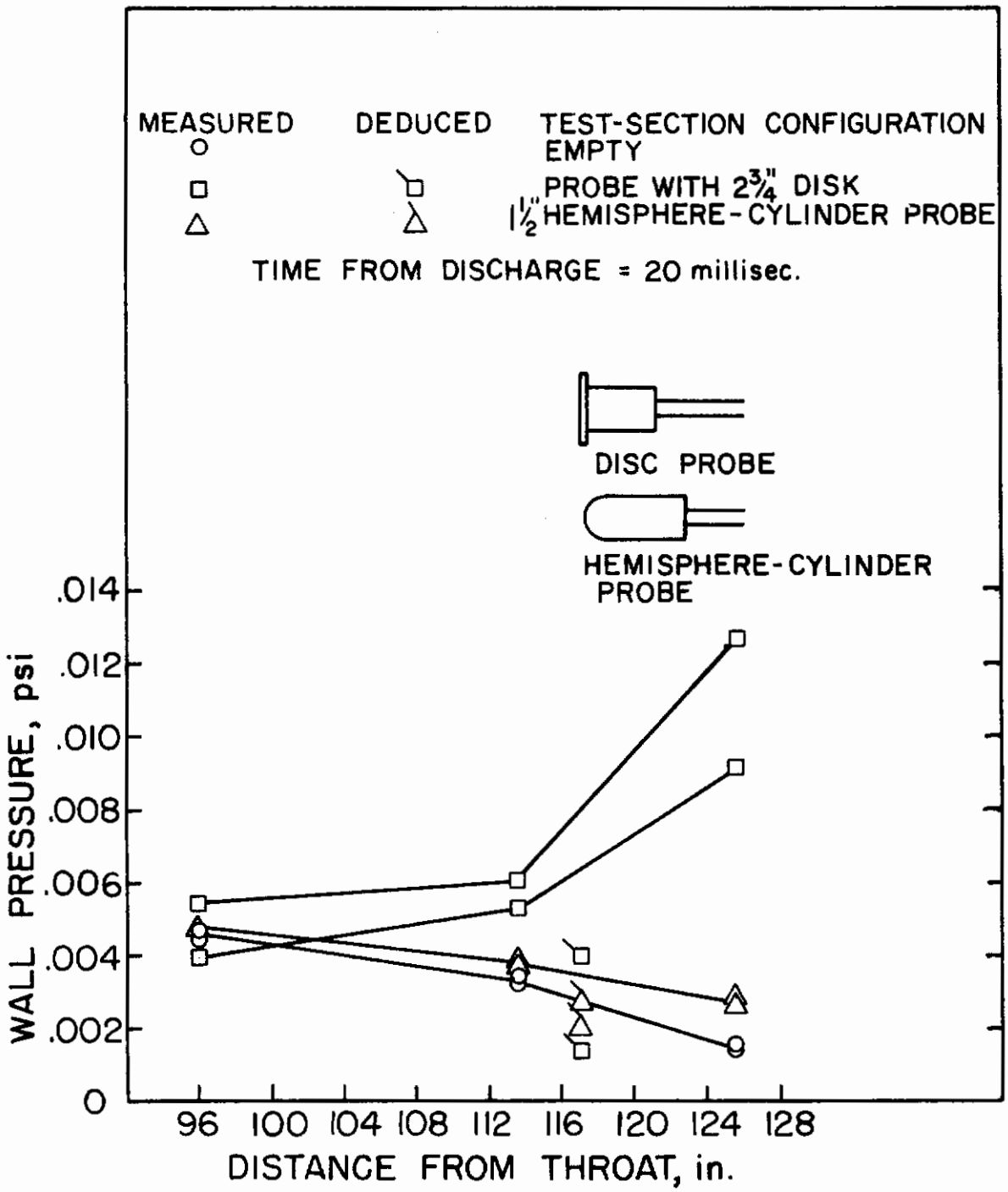

Fig. 12 Model Effects on Longitudinal Wall Pressures

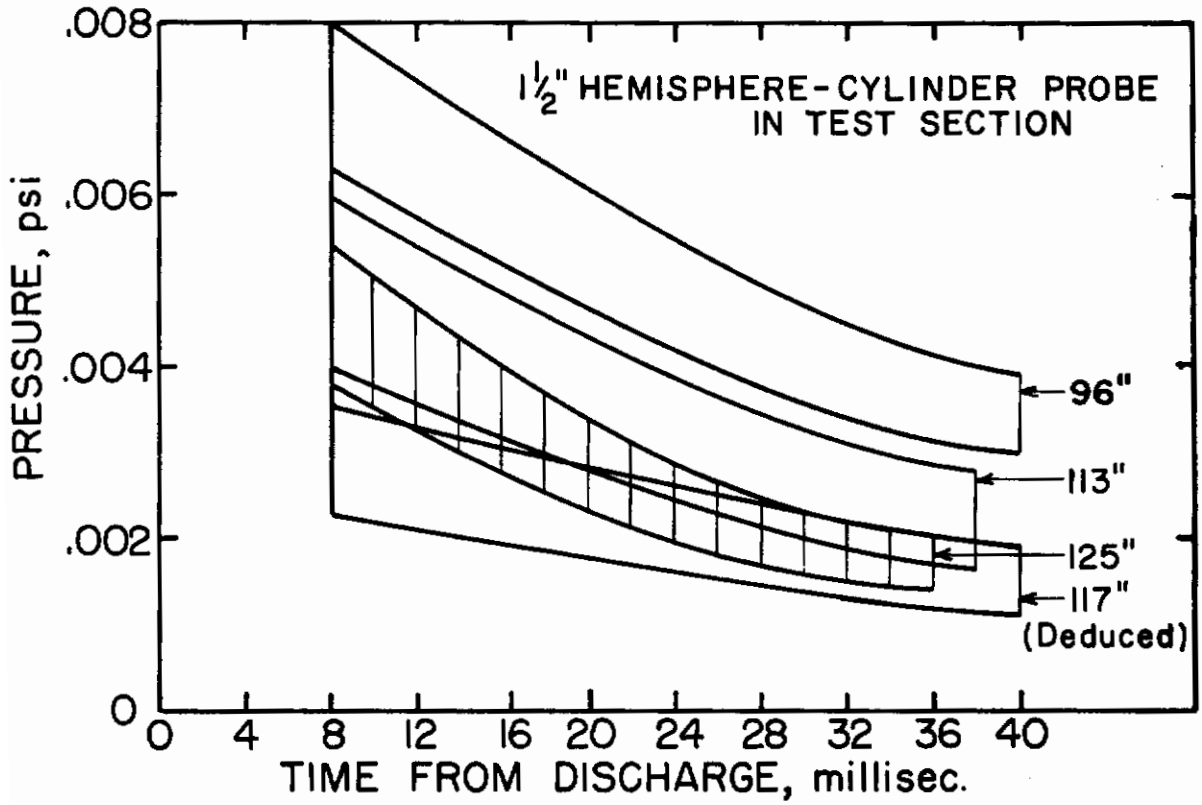

Fig. 13 Range of Static Pressures in the Test Section for 10 Nominally Identical Runs

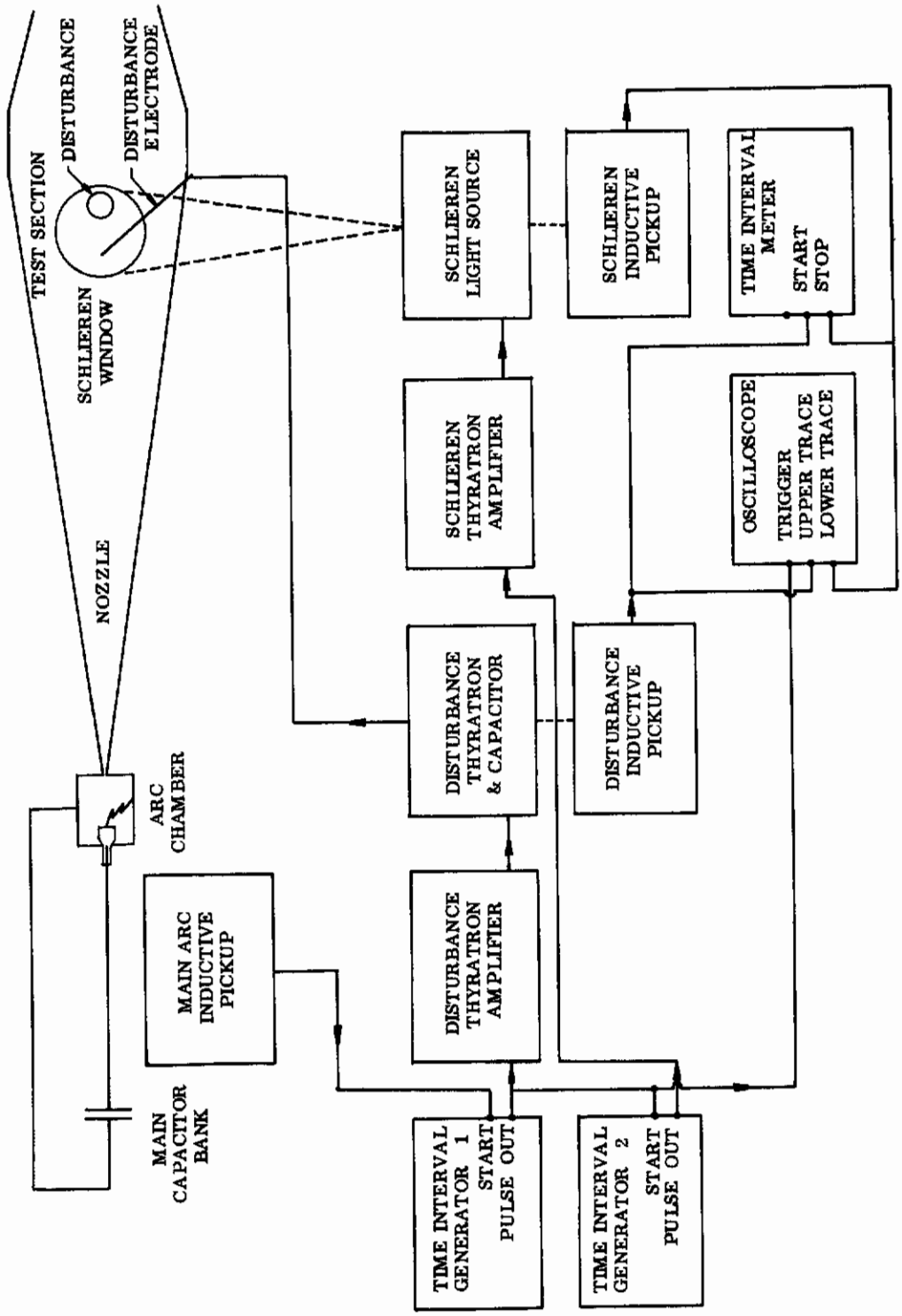

Fig. 14 General Layout of System for Schlieren Measurements

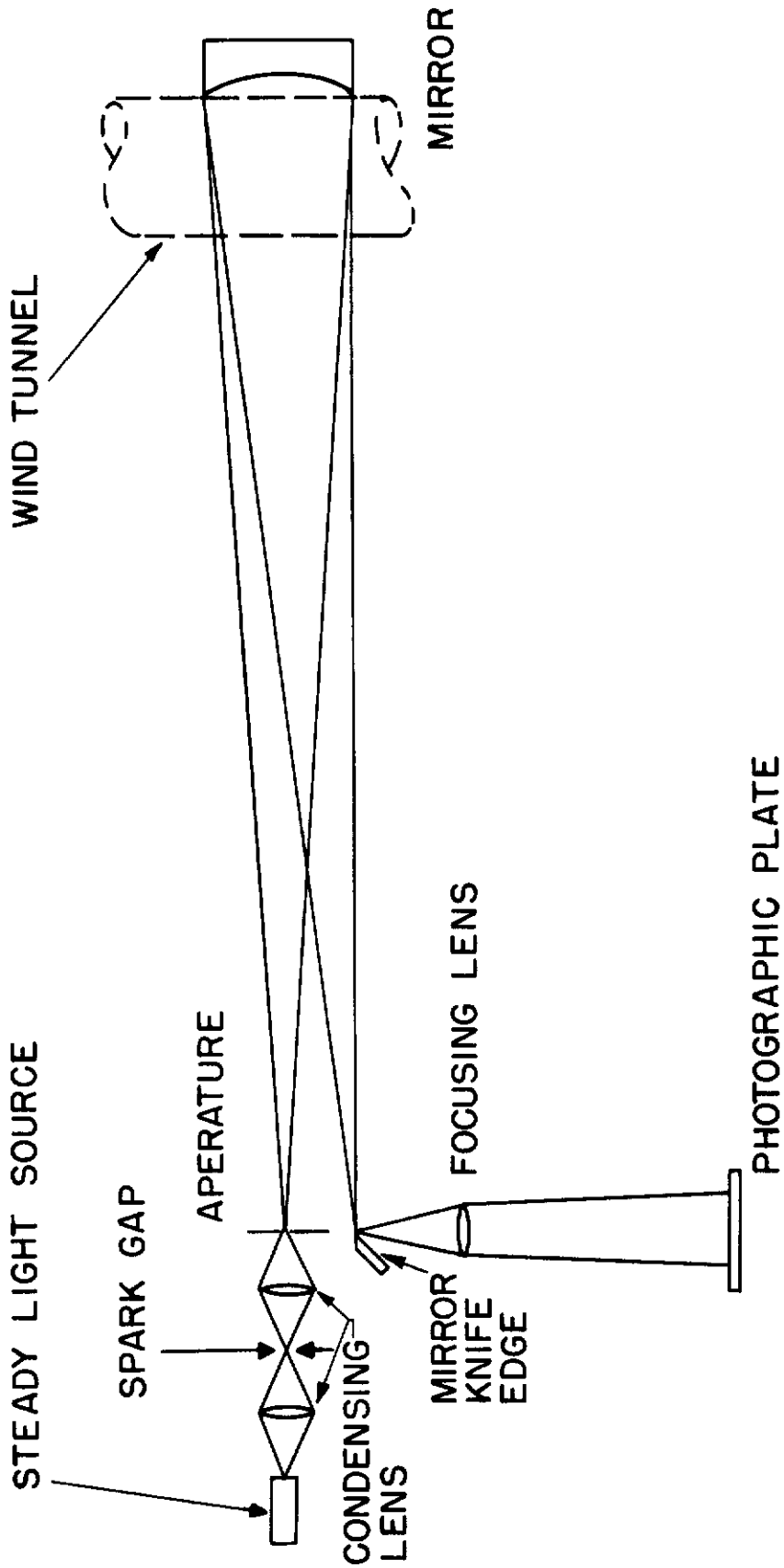

Fig. 15 Double-Pass Schlieren System

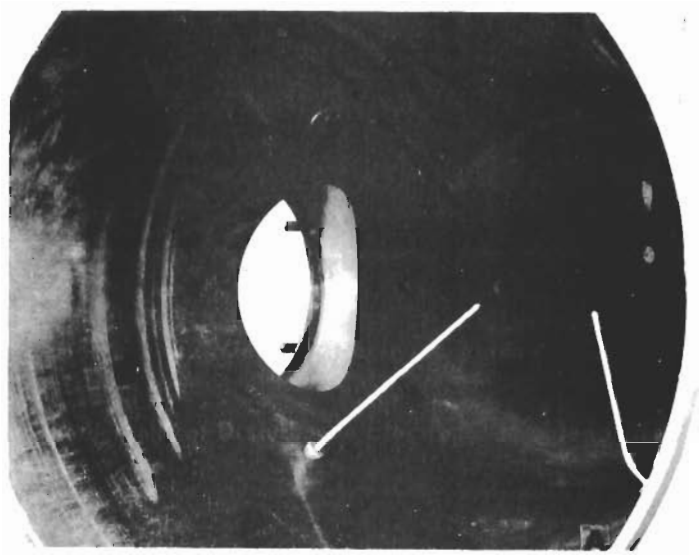

a. View from Diffuser, Looking toward Nozzle Throat

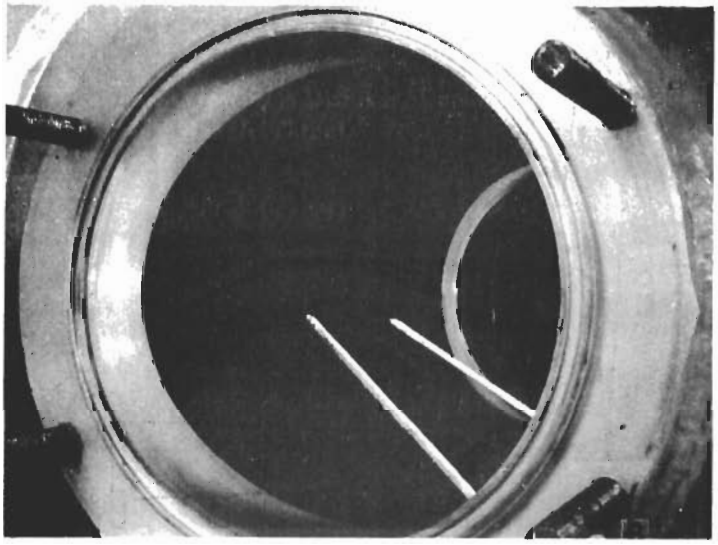

b. View from Schlieren Window

Fig. 16 Photographs of Disturbance Electrodes Mounted in Test Section

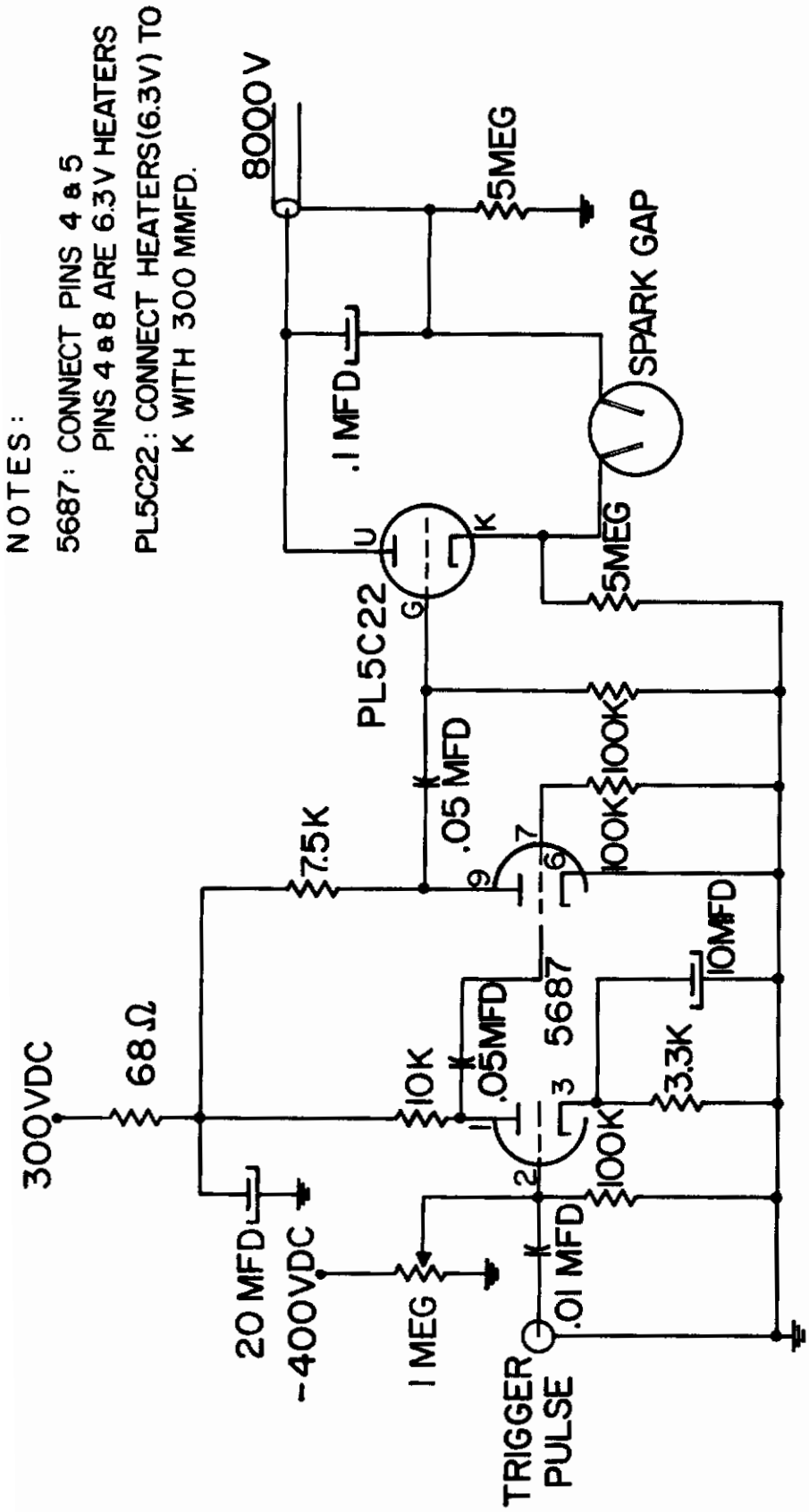

Fig. 17 Disturbance-Spark Circuit

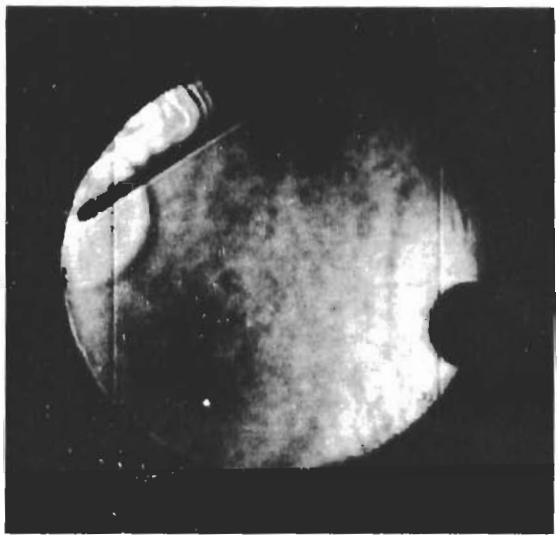

a. Disturbance with no Flow

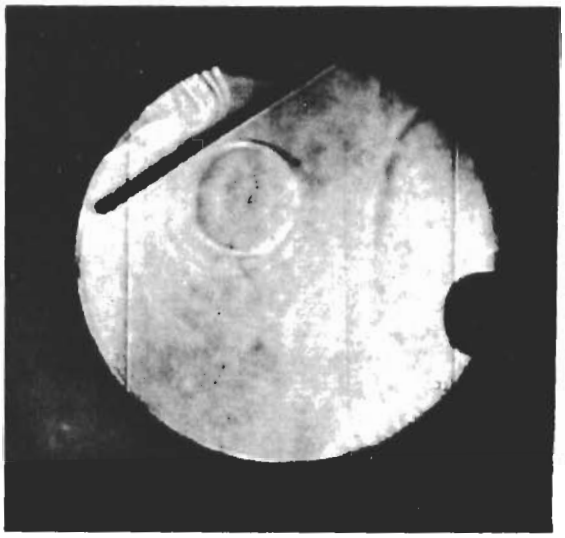

b. Disturbance with Flow

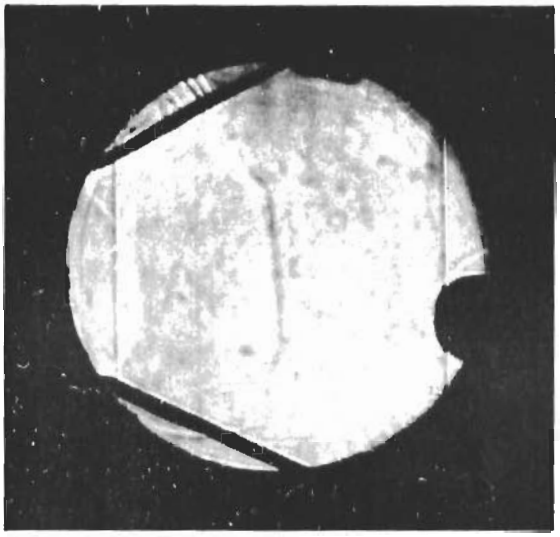

c. Plan View of Disturbance with Flow

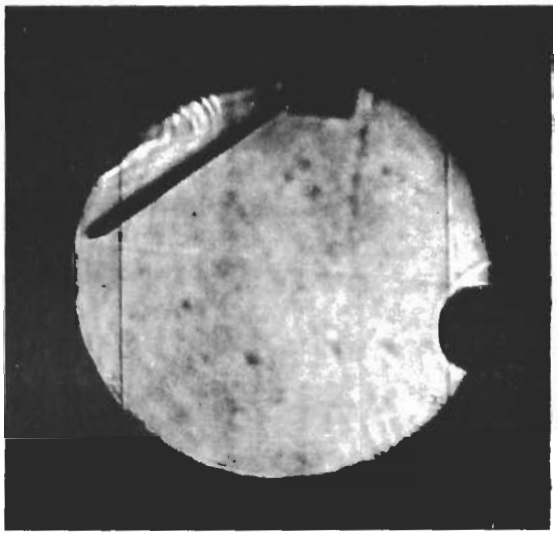

d. Electrode Wake

Fig. 18 Schlieren Photographs

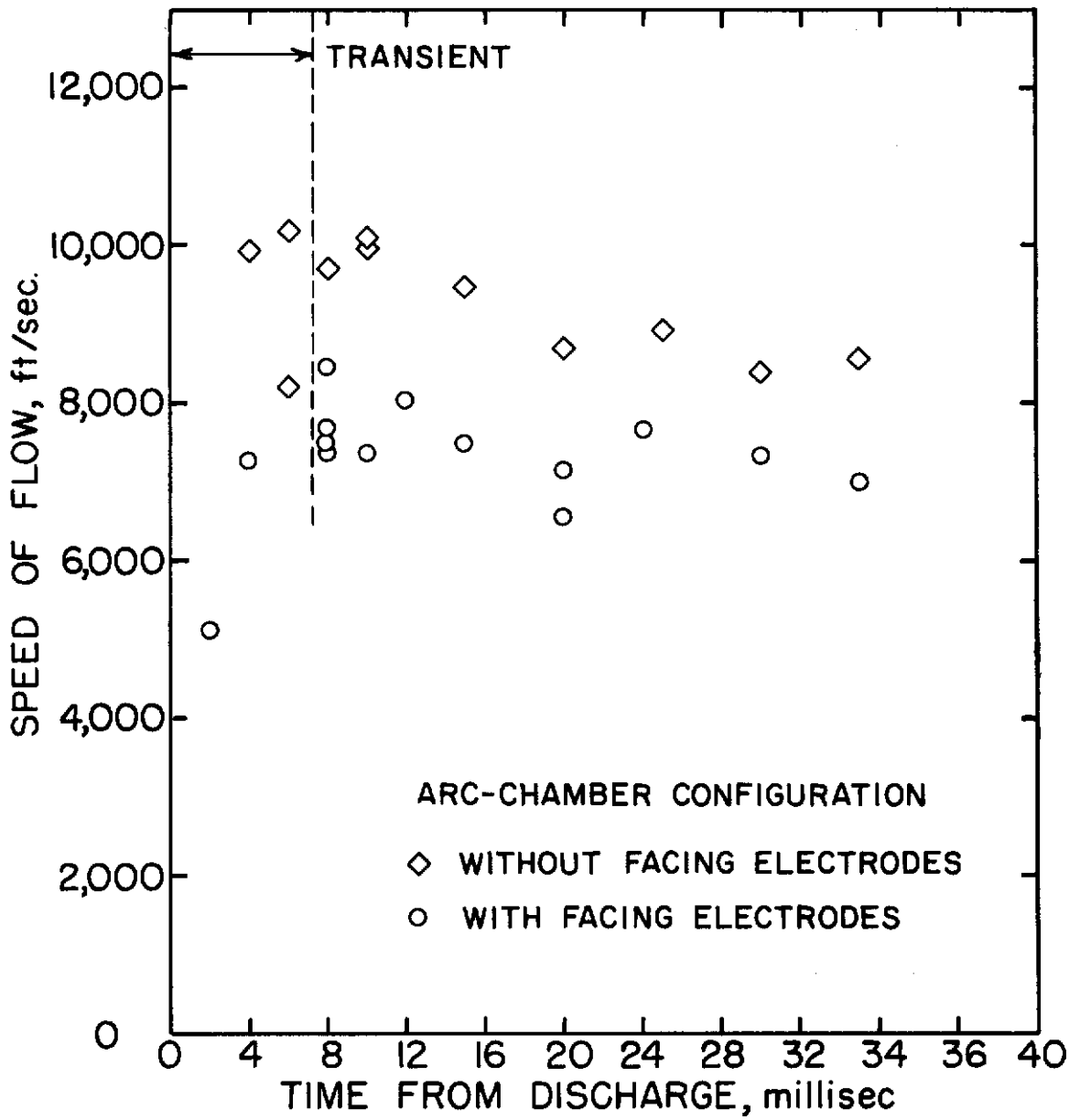

Fig. 19 Measured Speed of Flow

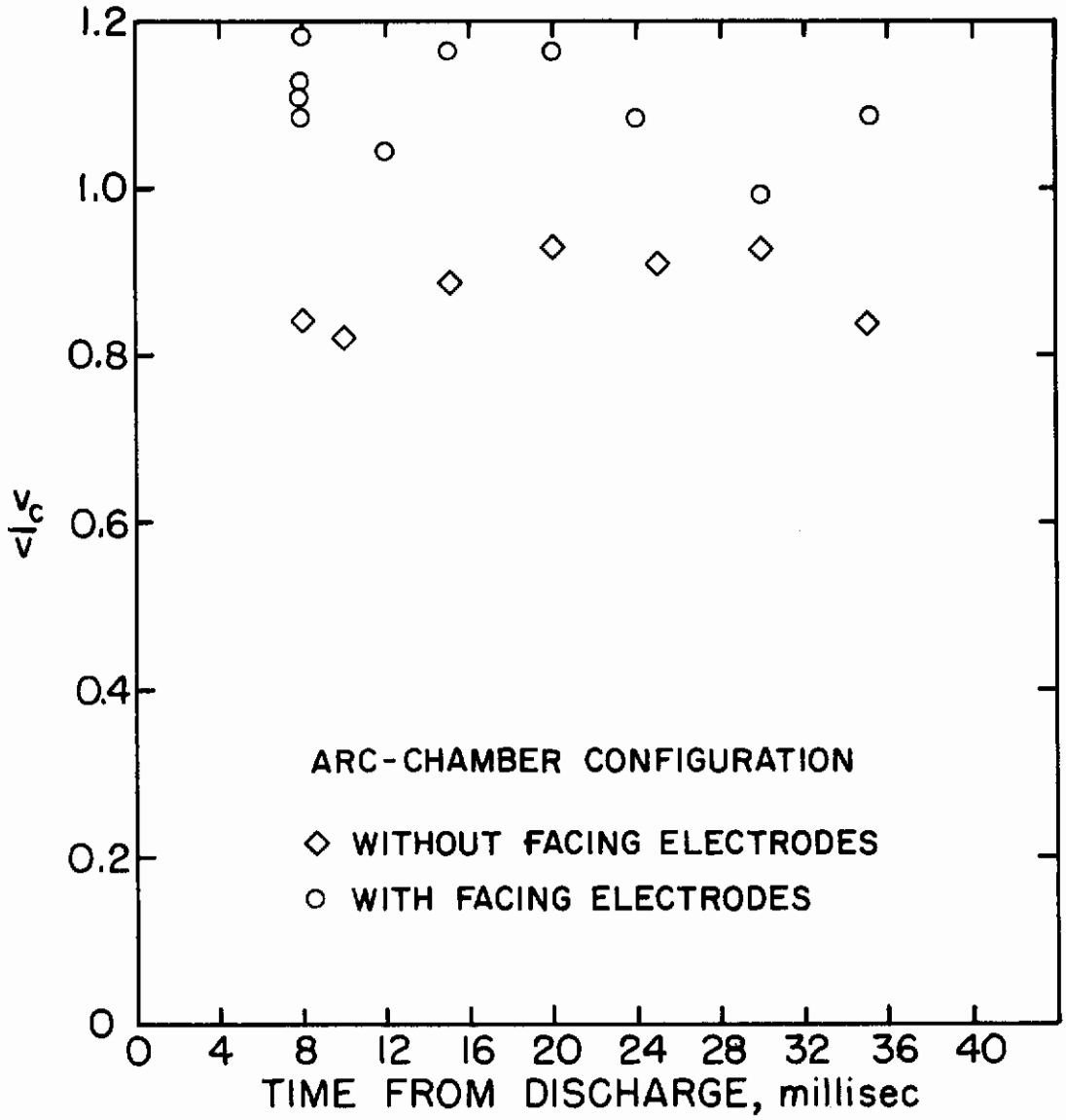

Fig. 20 Comparison of Calculated and Measured Speeds of Flow

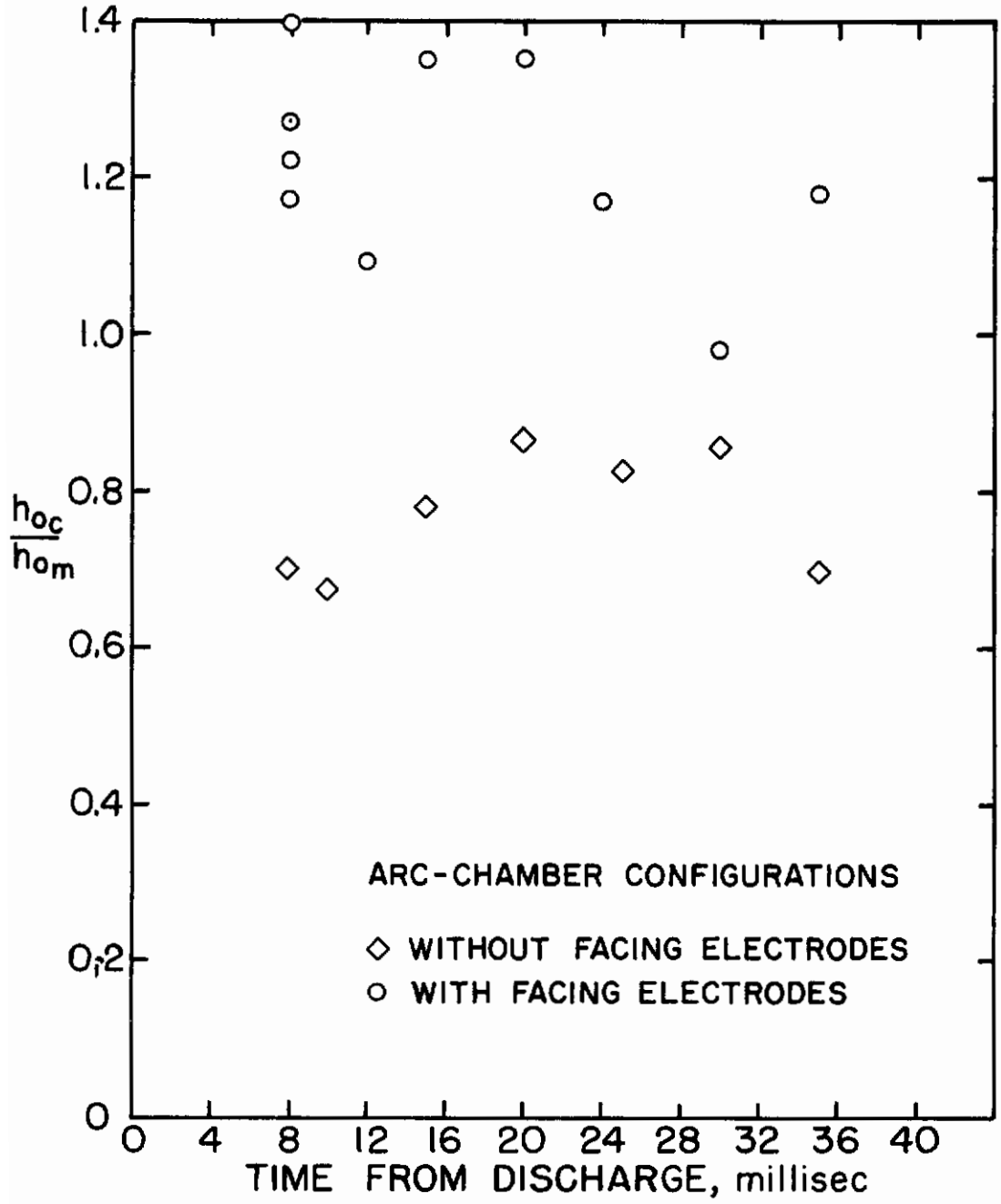

Fig. 21 Comparison of Calculated and Deduced Stagnation Enthalpies